Salinity-driven changes in *Salicornia* cell wall nano-mechanics and lignin composition

Stefany Cárdenas Pérez[a,*], Janusz Strzelecki[b], Agnieszka Piernik[a], Ahmad Rajabi Dehnavi[a], Paulina Trzeciak[c], Radosław Puchałka[c], Agnieszka Mierek-Adamska[d,e], Jorge Chanona Perez[f], František Kačík[g], Vladimír Račko[g], Ján Kováč[h], Samarthya Bhagia[i], Jaroslav Ďurkovič[h],

[a] Department of Geobotany and Landscape Planning, Faculty of Biological and Veterinary Sciences, Nicolaus Copernicus University in Torun, Lwowska 1, 87-100 Toruń, Poland

[b] Institute of Physics, Faculty of Physics, Astronomy and Informatics, Nicolaus Copernicus University, Grudziadzka 5, 87-100, Torun, Poland

[c] Department of Ecology and Biogeography, Faculty of Biological and Veterinary Sciences, Nicolaus Copernicus University, Lwowska 1, Toruń, 87-100, Poland

[d] Department of Genetics, Faculty of Biological and Veterinary Sciences, Nicolaus Copernicus University, Lwowska 1, 87-100 Toruń, Poland

[e] Centre for Modern Interdisciplinary Technologies, Nicolaus Copernicus University, Wileńska 4, 87-100 Toruń, Poland

[f] Departamento de Ingeniería Bioquímica, Escuela Nacional de Ciencias Biológicas, Instituto Politécnico Nacional, Av. Wilfrido Massieu, Esq. Manuel L. Stampa s/n, 07738, Gustavo A. Madero, Ciudad de México, Mexico

[g] Faculty of Wood Science and Technology, Technical University in Zvolen, 96001 Zvolen, Slovakia

[h] Faculty of Forestry, Technical University in Zvolen, 96001 Zvolen, Slovakia

[i] Biosciences Division, Oak Ridge National Laboratory, Oak Ridge, Tennessee 37831, United States

Abstract

Widespread increases in soil salinisation significantly reduce agricultural lands. Still, salt-tolerant plants, such as *Salicornia europaea* L., can play a crucial role in the reclamation of these lands, especially for the cultivation of crops. During the last few years, scientists have reported that anatomical modifications in *S. europaea* enable the plant to prevent damage caused by high soil salinity. However, there is limited knowledge about their biophysical cell responses under salt adaptations. It is essential to meet the world's demand for sustainably produced biomass for food and the growing bio-products sector.

We consider the potential of *S. europaea* to mitigate soil salinisation and its application in agriculture by utilising all fractions of the produced biomass and producing value-added food, feed, bio-compounds and bioenergy. This work investigates how different salinities induce significant anatomical and biophysical changes in the plant. These changes include cell size and shape variations, lignin polysaccharide distribution and composition, gene expressions (such as *NHX1* and *SOS1*), and their correlation with cell wall elasticity (CWE). Understanding these adaptations and identifying the best salt level for *Salicornia* growth is critical for maximising the yield and quality of these plants and comparing them with other crops.

The effects of salinity on *S. europaea* stem cells of plants grown under salinity levels ranging from 0 to 1000 mM NaCl were assessed and correlated through several parameters. These included directly measuring CWE in-vivo using an atomic force microscope (AFM), studying the shape and size of water-storing parenchyma cells, analysing xylem cell wall lignification and lignin monomer composition, examining the presence of calcium oxalate crystals inside cells, and monitoring the expressions of salt-related genes (Se*NHX1* and Se*SOS1*).

AFM revealed that salinity stimulated increased CWE, which we interpreted as the cell's turgor conservation effect. Direct values of the cell wall stiffness subjected to salinity were obtained, with Young's modulus ranging from 0.52 to 0.03 MPa. Plant cells under 400 and 1000 mM NaCl swelled 3.5

and 5.4 times, respectively. These findings indicate significant structural changes in response to salt stress, which may have implications for future studies of crop cultivation in saline environments.

The most relevant structure-function changes observed included increased CWE, thickening of palisade tissue, water-storing parenchyma, and pith cylinder. Furthermore, we identified increases in the lignified xylem, large calcium oxalate crystals, and Se*NHX1* gene expression significantly expressed at higher salinity levels. The high S/G ratio in lignin for 0–400 mM NaCl may have influenced the rigidity and hydrophobicity of the cell walls, which is relevant for agriculture applications and plant-breeding strategies.

Salicornia cells exhibit multiple biophysical adjustments to tolerate salt stress, making them an attractive candidate as an intercropping halophyte in saline soils. The strong correlation between CWE and the water-storing parenchyma cell's area, xylem vessel diameter/thickness, and Se*NHX1* gene expression supports a physiological adjustment to survive in very high-salinity conditions, making these parameters valuable stress markers in crop breeding programs.

The unique properties of the *Salicornia* cell walls studied in this research could potentially inspire the development of new materials with enhanced mechanical elasticity and resistance to osmotic stress. Additionally, the insights gained in this study can be applied in future research aiming to produce biomass or to improve the salt tolerance of other crop plants, which is a significant challenge in agriculture, particularly in arid and coastal regions.

1. Introduction

The increase in salinisation in agricultural lands is a significant factor adversely affecting productivity and food security due to its essential reduction in lands that can be classed as arable. According to the FAO, 2022 (Soil salinity | Global Soil Partnership, FAO), soil salinisation takes as much as 1.5 million ha of farmland out of production each year. The annual loss in agricultural productivity is estimated at up to USD 31 million. Therefore, there is an essential need to increase crop production from degraded natural

lands by supporting the restoration of the productivity of lands and ecosystems. High salinity disturbs plants, especially glycophytes, by affecting their intracellular ion homeostasis, causing a dysfunction in cell walls and membranes, a decrease in metabolic activity, loss of turgid cells, a disruption of electrostatic forces, and other effects that inhibit growth and development (Li et al., 2022; Yadav et al., 2012).

On the other hand, those plants that have evolved to be salt tolerant, known as "halophytes", are capable of modifying some traits in their physiology and biophysical structure depending on the environmental conditions with an increase in salinity (Flowers and Colmer, 2008; Koyro, 2006). An important halophyte is *Salicornia europaea* L. (Chenopodiaceae), which is considered one of the most salt-tolerant plants (Cárdenas-Pérez et al., 2021; Lv et al., 2012). It has recently attracted the attention of many investigations due to its potential for desalination and reclamation of degraded lands and its numerous applications in ecology (e.g., aquaculture, phytoremediation), agriculture, food, pharmacy, chemical and cosmetic industries, as well as applications as a bioenergy crop thanks to its seed's oil and biomass content for biofuel or bioethanol production (Cárdenas-Pérez et al., 2021).

This species usually adjusts osmotic balance inside its cells by pumping Na^+ ions out of the membrane by accumulating inorganic ions in vacuoles or sending them to the apoplast (Barragán et al., 2012). Other mechanisms also contribute; for instance, according to Yadav et al.(Yadav et al., 2012), *Salicornia* species use antiporters to regulate the ion homeostasis in plant cells to quickly adapt to salinity. *NHX1* and *SOS1* proteins are widely regarded as key players in the sequestration and efflux of sodium (Na+) in plant cells to avert ion toxicity in the cytosol under salinity stress. It has been reported that *NHX1* antiporter present in tonoplast is in charge of pumping Na^+ into the vacuole, while *SOS1* in the plasma membrane is pumping Na^+ into the apoplast (Chen et al., 2014; Fan et al., 2013; Lv et al., 2012; Shi et al., 2002) (Fig. S1), due to these and other mechanisms, *S. europaea* cytoplasm and organelles are protected and cells can remain turgid while surviving in a saline environment.

However, cell architecture remodelling should also take place to maintain a high cell turgidity when subjected to salinity. Cell size and cell wall elasticity (CWE) are traits that may contribute to a plant's salt

tolerance and are considered by some authors to be important mechanisms of adaptation to salt or drought stress (Cárdenas-Pérez et al., 2022; Hessini et al., 2009; Martínez et al., 2007). Chimenti et al., (2006); Martìnez et al., (2004) have reported that maintaining turgor is essential for keeping normal cell functions that contribute to plant growth under low water activity. They have also identified that osmoregulation and CWE traits may help to maintain symplast volume and turgor pressure inside cells. These have been reported in several species as responses to abiotic stress (Forouzesh et al., 2013; Kim and Lee-stadelmann, 1984; Patakas et al., 2002). Other authors (Marshall et al., 1999; Martínez et al., 2007) indicate that salt-sensitive plants subjected to dehydration may maintain their cell turgor via cell shrinkage, this helps to avoid turgor-loss volume and this is somehow associated to primary cell walls, which are complex and dynamic systems capable of deformation due their intrinsic viscoelasticity (Fradera-Soler et al., 2022).

Meanwhile, Boughalleb et al., (2009); Debez et al., (2006); Rozentsvet et al., (2022) reported that the water storage parenchyma and cell volume increase in succulent halophytes under high salinity, which has drawn much attention in recent years. However, there is little knowledge about cell-wall stiffness modifications in halophytes under increasing salinity. Additionally, the presence of big calcium oxalate crystals in *S. europaea* is also not clearly understood. These crystals may help survive under high salinity, working as dynamic carbon pools, aiding the plant in photosynthesising under salt-stress conditions, especially when water losses are crucial. So, *S. europaea*, which survives at high salinities, may use carbon dioxide from crystal decomposition instead of from the atmosphere, as proposed by Tooulakou et al., (2016).

Many physiological phenomena associated with salinity tolerance are related to anatomical structure-function changes. According to Hameed et al., (2010) such changes are mainly stem succulence, well-developed water-storing tissues in the cortex, increases or decreases in xylem vessel number, xylem cell wall thickening and lignin composition. Lignin plays a vital role in the growth and development of plants and can be linked to cell wall stiffness. As a complex phenolic polymer, lignin may enhance plant cell wall rigidity and hydrophobic properties. It promotes mineral transportation through the vascular bundles

and provides mechanical strength when the water-storing tissue is strongly developed. Besides other critical biological functions, lignin can reduce both, water penetration into plant cell walls and transpiration, and thus it assists in maintaining cell osmotic balance and protective membrane integrity under conditions of high salt stress (Grigore and Toma, 2020; Liu et al., 2018; Schuetz et al., 2014). Thus, defining the chemical characteristics of plant cell walls is of great importance for bioprocessing, to utilise specific fractions of the produced biomass or to evaluate the results of plant breeding and/or responses of plants under stressful abiotic and biotic factors (Liu et al., 2018).

However, it has emerged from many studies that not all plants use the exact general salt tolerance mechanisms (Xiong and Zhu, 2002); for example, cell size and polysaccharide composition changes in response to abiotic stress are known to occur differently between species. For this reason, there is a growing interest in researching the structural and biophysical changes of halophytic species to understand more deeply their salt-tolerance mechanisms.

According to Tester and Davenport, (2003) , most halophytes can store significant quantities of Na^+ in their cells of stem without adverse effects. For instance, Lv et al., (2012) demonstrated that *S. europaea* can accumulate a maximum of approximately 300 mg g^{-1} dry weight of Na^+ when grown under 800 mM NaCl, and it shows growth stimulations even upon further NaCl addition. According to these authors, the relative weight of Na^+ was highest in the stems' water-storing parenchyma, followed by the palisade tissue, and the lowest value was detected in the pith cylinder. Their results also indicate that *S. europaea* predominantly accumulates Na^+ into the vacuoles.

As it is known, structure properties related to plants can be studied at different levels, such as spatial variability of tissues at the macroscale, size and shape at the microscale, and the structure and composition of cell walls and middle lamella at sub-micro- and nano-scales. In contrast, individual polysaccharide structures and linkages in cell walls can be considered at the nano-scale (Zdunek and Kurenda, 2013). Therefore, analysis of nano-mechanical properties through atomic force microscopy (AFM) allows us to determine physical cell-wall characteristics *in vivo* by determining Young's modulus (*E*). This parameter

characterises the behaviour of an elastic material at a nano-metric scale (Cárdenas-Pérez et al., 2016). Thus, the CWE of cells can be estimated by determining *E*, where the lower the *E*, the higher the CWE. To date, plenty of studies have focused on mechanical properties at macro scale, but only a few studies have performed research at the micro- and nano-scale levels. To the best of our knowledge, this is the first time such research has been conducted on the mechanical properties of *in-vivo* cell walls in *S. europaea*. This is probably due to the lack of suitable technology to perform mechanical manipulation at such a length scale (Zdunek and Kurenda, 2013). Study of the micro- and nano-mechanics of plants is essential since the composition at this level is very dynamic, such as during high-salinity stress responses. Moreover, cells are the primary units in charge of the mechanical performance of the entire plant. Thus, they are considered to be the starting point for structure-function studies related to biomechanical models.

Many studies focus on the adaptation of a single or small number of traits, but there is still a lack of research taking into account the complexity of salt tolerance (Cárdenas-Pérez et al., 2022). Thus, the present study tracked: changes in the biophysical structure-function in cell wall elasticity, cell size and cell shape; thickening of stem cross-sections; thickening of the diameter and cell walls of xylem vessels; changes in lignin monomer composition; and variations in calcium oxalate crystals. These parameters were examined inside the cells of *S. europaea* against different salt levels to elucidate their correlations and clarify how their cell's mechanical properties, such as CWE (considered to be one of essential physiological mechanisms of adaptation to water stress) contribute towards the plant's enhanced salt adaptation. Because the perception of salt stress and how such perception results in suitable responses need further exploration. In this context, sensing plant cell walls is crucial, detecting and initiating adaptive responses to salt stress (Colin et al., 2023).

We hypothesised that subjected to different salinities, *S. europaea* undergoes critical structural changes such as increases or decreases in cell wall elasticity, cell size and modifications to shape. At the same time, xylem lignification may be enhanced and changed in its composition. Variations in cells' calcium oxalate crystal elements may also be distinguished, where we expect that, under high salinity,

bigger calcium oxalate crystals will be present. Also, variations in the expression of *NHX1* and *SOS1* genes can be projected to cope with salinity without suffering significant damage. Therefore, we designed this study to bring in a new structural approach through atomic force microscopy (Fig. S1) to develop the biophysical characterisation of *Salicornia* cells complemented with identification of elemental composition and distribution through scanning electron microscopy–X-ray spectroscopy and X-ray micro-computed tomography; this will open a new perspective on the structure-function relationships of *S. europaea* cells concerning salinity and thereby reveal contrasts between physiological traits and responses.

2. Materials and methods

2.1 Plant growth conditions and salt treatments

We collected *Salicornia* seeds in Poland at Inowrocław-Mątwy (52°48′N, 18°15′E), which is a salt land associated with waste from a soda ash and chemical factory that affects the local environment with a salinity of ~55 dS m^{-1} (~550 mM NaCl). The seeds were germinated and grown according to the steps reported by Cárdenas-Pérez et al. (Cárdenas-Pérez et al., 2020; Cárdenas-Pérez et al., 2022) with a slight modification in salt treatments at 0, 200, 400, 600, and 1000 mM NaCl. We cultivated 60 plants under five treatments (12 plants per treatment). After 60 days under salt treatments, nano-mechanical properties, structure-function analysis, xylem lignin identification and composition, cell X-ray elemental analysis and scanning electron microscopy (SEM) observations were carried out. For all the performed studies, the samples were collected through cross-sections made on the same level of the stem for each analysed individual respectively.

The collection of plant material complies with relevant institutional, national, and international guidelines and legislation, the *IUCN Policy Statement on Research Involving Species at Risk of Extinction* and the *Convention on the Trade in Endangered Species of Wild Fauna and Flora*. The voucher specimen of the plant material has been deposited in the publicly available herbarium of the Nicolaus Copernicus University in Toruń (Index Herbarium code TRN). The deposition number is not available (Dr hab. Agnieszka Piernik, Prof. NCU, formally identified plant species, and permission to work with the seeds

was provided by the Regional Director of Environmental Protection in Bydgoszcz, WOP.6400.12.2020.JC).

2.3 Morphometry of S. europaea stems cells by image analysis

From the fleshy segment stem of the middle primary branch of *S. europaea* plant treatments (0, 200, 400, 600, and 1000 mM NaCl) (Fig. S2), thin slices (0.5 mm) of fresh tissue were obtained using a bi-shave razor blade following the steps reported by Cárdenas-Pérez et al. (Cárdenas-Pérez et al., 2022). They were observed through a light microscope (LM) (Olympus BX51, USA) and a digital camera (DP72 digital microscope camera). The Area (A), major diameter (mD), aspect ratio (AR) and roundness (R) parameters were obtained from the fresh stem-cortex cells of the water-storing parenchyma. The LM images were captured at a magnification of 10×/0.30 in RGB scale and stored in TIFF format at 1280×1024 pixels. A total of 300 ±50 cells from 12 individuals per treatment were analysed. Image analysis (IA) was performed in FIJI ImageJ v. 1.47 (Schindelin et al., 2012). The A was estimated as the number of pixels within the boundary, the mD was determined by the distance between the two points separated by the largest coordinates in different orientations of the cell cross sectional area. Then, the AR is the quotient between the minimum and major diameter, i.e. a value of 1.0 results for equidimensional objects, and AR → infinity for extended objects. R was found through the equation $R=(4\ A)/(\pi\ (mD)^2$, where a perfectly round object will have R = 1.0 while more elongated objects will show an R → 0. Later, thickness measurements of the three analysed regions (edge, middle and centre) were obtained through the straight ImageJ tool, which displays the number of pixels within the boundary, and converted to metric units.

2.4 Nano-indentation with AFM

2.4.1 Sample preparation for nano-indentation

Salicornia europaea plants grown under 0, 200, 400, 600, 1000 mM NaCl concentrations were evaluated. The cross-section slices of stem with approximately 0.5 mm thickness were cut using a razor blade,

maintaining a flat and parallel cutting plane as much as possible. A section from each plant was attached with a compound resin in a plastic 60 mm Petri dish and kept in distilled water.

All nano-indentation measurements were performed with Bruker (former Veeco) Bioscope 2 atomic force microscope. Cantilevers used were tipless MLCT-O10, probe from Bruker (AFM Probes - MLCT-O10, n.d.). Colloidal probes were prepared with polystyrene beads (25 μm diameter) attached with epoxy glue Plus, following protocol (Nanowizard, n.d.). Cantilevers were calibrated using the thermal tune method (Hutter and Bechhoefer, 1993) in liquid before each measurement session. Deflection sensitivity was determined on a dedicated hard gold evaporated glass substrate. Thus, the indentation (δ) is zero, and the piezoelectric displacement (z) is the deflection sensitivity (def.s.) according to $z = \delta$ + def.s. Then, the def.s. is expressed in nm/V. In the present analysis, the calculated def.s. was 28.1 ± 0.2 nm/V and the spring constant (k) 0.236 N/m.

All examinations were performed within Petri dishes. An optical microscope was used to place an AFM cantilever in the desired spot. In each section, three testing regions were targeted: palisade tissue, water-storing parenchyma and pith parenchyma. Hereafter in this study, these regions will be called “edge”, “middle” and “centre”. At each region, more than five spots were selected for nano-indentation, depending on the sample’s topography. Within 10 μm of such a spot, more than 30 force curves were obtained from the same region. Significant variations in sample topography often limited the number of force curves that could be successfully measured with 15 μm vertical range of the Bioscope 2 scanner. A relative force trigger >100 nN, force-separation curves and Young’s modulus (*E*) estimation were performed in NanoScope Analysis software (Bruker, USA) as reported previously (Cárdenas-Pérez et al., 2018, 2016).

2.4.2 Cell nano-indentation along the three regions of *Salicornia* stem

In total, over 1000 valid force curves were obtained. The Young’s modulus (*E*) of each sample was obtained from the retracting force-indentation depth curve through Hertzian contact mechanics. Figure 1a shows the AFM nano-indentation through the cross-section of *S. europaea* stems; Figure 1b shows the

AFM tip exerting force on *Salicornia* turgid cells; and Fig. 1c shows a typical force curve obtained when indenting with colloidal probe.

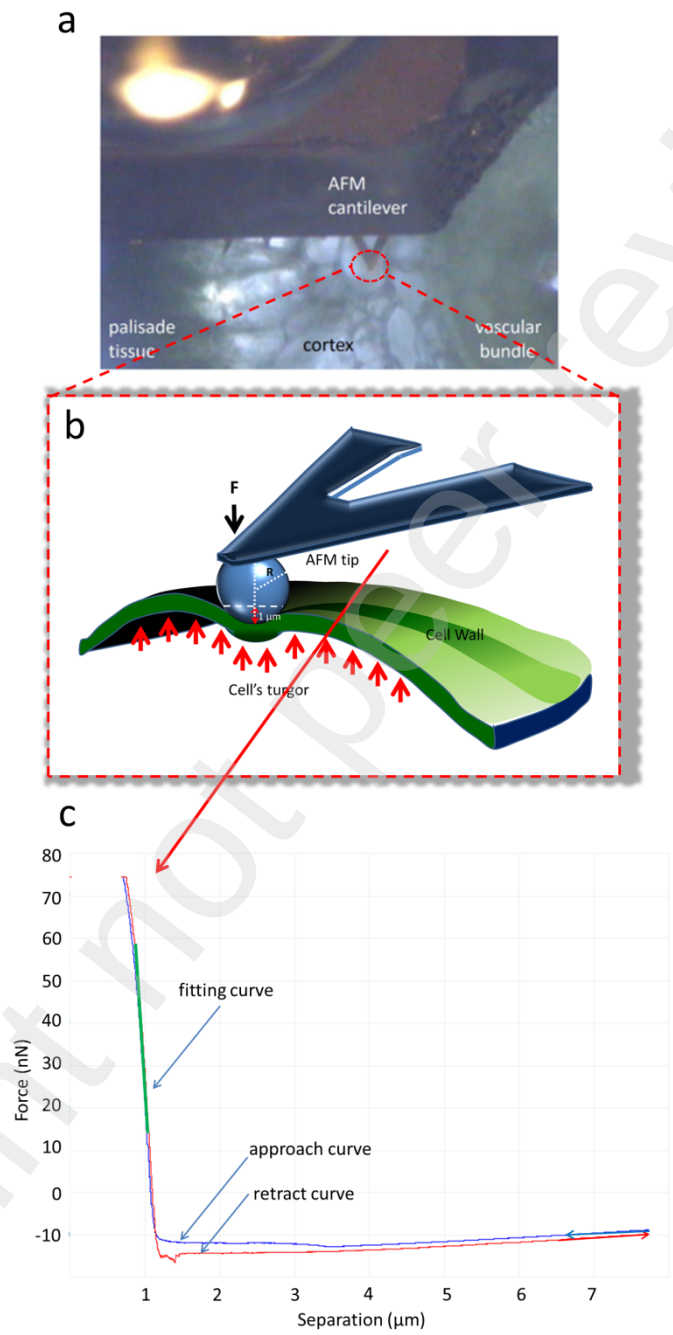

Figure 1. AFM nano-indentation through *S. europaea* cross-section stem. Tip positioning with optical microscope (a), depicted image of the tip exerting force by means of AFM, to the turgid cells (b) and

example of typical approach (blue) and retract (red) force curves obtained when indenting with colloidal probe (c)

According to Routier-Kierzkowska and Smith, (2013), when the indenter diameter is similar to or smaller than the cell wall thickness (~1 μm), the indentation can be influenced by global cell deformation. For these cases, sharper tips are usually used, which allow penetration of the cell among the cellulose micro fibrils. However, the present work aimed to produce relatively large indentations to evaluate the elasticity in *Salicornia* cells subjected to salinity. In this sense, an indenter bead (25 μm of diameter) for the analysis was selected; thus, the penetration through the polysaccharide matrix of the cells is avoided and it can be assumed that the cell wall is instead bent. Also, according to Zdunek and Kurenda, (2013) , when probing cells using a bead as the indenter, the cell's turgor is indirectly sensed, since it affects the measurements when the AFM tip exerts the force, because a large contact area causes flattening and bending of the cell wall in the place of indentation where turgor influences the measurements. Therefore, the obtained results of Young's modulus can be considered a convolution of the cell's wall elasticity (CWE) and the value of turgor inside the cells.

2.4.3 Determination of Young's modulus

Young's modulus (*E*) was calculated by fitting the Hertz model (Eq. 1) to the indentation slope of the obtained approach curves. An example of the force approach-separation curve obtained from the surface of *Salicornia* cells is shown in Fig. 1b.

$$F = \frac{4}{3}\frac{E}{(1-\nu^2)}\sqrt{R}\delta^{\frac{3}{2}} \quad (1)$$

where F = is force, E = Young's modulus, R is the indenter tip radius (12.5 μm), δ is indentation (nm) and ν is Poisson's ratio. The Poisson's ratio reported for elastic materials such as plant cells is usually between ν = 0.3–0.5 (Routier-Kierzkowska et al., 2012). For the evaluation of E, a value of ν=0.5 was used in all cases. Fitting of the model to experimental slope curves was performed using Nanoscope Analysis

software. The goodness of fit was verified using the determination coefficient (R^2) and it was decided to remove from further analyses curves with an R^2 lower than 0.8. So, E was obtained separately from each curve; their values are reported as the average and its corresponding standard error. Later, to study the distribution of E, the values were firstly plotted as histograms and fitted with an exponential distribution function model. The histograms were adjusted with a non-linear least squares regression analysis using the Marguardt–Levenberg algorithm. The purpose of this fitting procedure is to find the best-suited model to describe the distribution of E values of *S. europaea* cell walls exposed to different salinity concentrations.

2.5 Histological preparation of S. europaea tissues

The collected parts of the middle primary branch (see supplementary Figure S2) were placed in special cassettes to facilitate infiltration. The material was then transferred to a tissue processor (Leica TP1020) that had been adapted for material preparation using a Technovit7100 (Kulzer), which is a HEMA (2-hydroxyethyl methacrylate) -based embedding system. The first step of the whole process was fixation in FAA (40% formaldehyde – 10%, 70% ethyl alcohol – 85%, glacial acetic acid – 5%) for 24 hours. The entire process was carried out under vacuum pressure, increasing the infiltration quality of the tissue. Tissue fragments were dehydrated in increasing alcohol series (75–99.8%) for 2 hours per concentration. Then, the pre-infiltration was performed by soaking the samples in a mixture of Technovit7100 and alcohol in increasing proportions (1: 10; 1: 3; 1: 1) for 2 hours each, and the infiltration process was carried out with pure Technovit7100 for 6 hours. The polymerisation process takes place in two steps. The samples were fixed in resin with hardener I for 24 hours, after which they were placed in special embedding forms made of Teflon with a stainless-steel bottom (Kulzer technique). The samples were immersed in a mixture of Technovit7100 with hardener I and II. Kulzer's special patented design has been developed to keep the temperature in low ranges during polymerisation, to provide uniform hardening of the blocks and, thus, uniform and thinnest-possible cross-sections with an artefact-free tissue morphology. The blocks prepared in this way were cut into 4–6 µm sections on a Leica RM2235 rotary microtome with Leica TC-65 tungsten razor blades. After mounting on slides, they were stained with 1% toluidine blue

(Astral Diagnostic), phloroglucinol or basic Fuchsin dyes (dyes that allow the identification of lignin) and sealed with CitrateMountTM Medium (Polysciences). The samples were analysed and captured through a Leica DM 2500 LED light microscope equipped with a Leica DMC5400 digital camera and Leica Application Suite X (LAS X) software. Similarly, to the aforementioned LM image analysis of water-storing tissue cells, xylem diameter and cell wall thickness were calculated in those cross-sections stained for lignin identification at treatments 0, 400 and 1000 mM.

2.6 Scanning electron microscopy–X-ray microanalysis

For scanning electron microscopy, stem segments were fixed in glutaraldehyde and dehydrated in ethanol and acetone. Fresh stem sections were dried in liquid CO_2 using a Leica EM CPD030 critical point drier (Leica Microsystems, Wetzlar, Germany). For X-ray microanalysis, fresh stem sections were immediately frozen and freeze dried. All sections were mounted on specimen stubs, sputter-coated with gold in the Sputter Coater K650X (Quorum Technologies, Ashford, UK) in an argon atmosphere and examined with scanning electron microscope (SEM) and energy-dispersive X-ray (SEM-EDX) spectroscopy under high-vacuum conditions. SEM-EDX observations were performed using an SEM (JSM-6390 JEOL, Tokyo, Japan), operating at 20 kV and working distance 12 mm, equipped with an EDX spectroscope INCAx-act (Oxford Instruments, Abingdon, UK). The microanalysis was carried out in cell walls and/or lumens of cortex cells on transversal surfaces of three specimens per treatment 0, 400 and 1000 mM NaCl, with 3–6 measurements.

2.7 X-ray micro-computed tomography

Stem segments of 0 and 1000 mM NaCl of approximately 0.8 cm in length were dried in a CO_2 environment using a critical point drier. X-ray micro-computed tomography imaging was performed with a Phoenix V|Tome|X L 240 device (GE Sensing & Inspection Technologies, Wunstorf, Germany) as described in detail by Karadžić et al. (Karadžić et al., 2020). The three-dimensional datasets were

evaluated using VGSTUDIO MAX 2.2 software for industrial computed tomography data (Volume Graphics, Heidelberg, Germany).

2.8 Analysis of lignin monomer composition

The analysis of nitrobenzene oxidation (NBO) products was performed in the extracted stem biomass. Water- and ethanol-soluble extractives were determined using a standard analytical protocol developed by the National Renewable Energy Laboratory, USA (Sluiter et al., 2008). Alkaline NBO was carried out in stainless-steel vessels using a modified method of Kačíková et al., (2020). An amount of 200 mg of extracted biomass was reacted with 5 ml of 2 M NaOH and 0.4 ml of nitrobenzene at 180 °C for 2 h. Then the vessels were immediately cooled in cold water. The excess of nitrobenzene was twice extracted with dichloromethane, and the organic phase was removed. The aqueous phase, acidified by 2 M HCl to pH around 2.5, was extracted with dichloromethane thrice. Then the organic phase was collected and dried with anhydrous sodium sulphate, gently evaporated in a nitrogen stream, and dissolved in methanol. NBO products were analysed by high-performance liquid chromatography using an Agilent 1200 apparatus (Agilent Technologies, Santa Clara, CA, USA) equipped with a diode array detector at 240 nm, and a Kinetex C18, 2.6 µm, 150×4.6 mm column (Phenomenex, Torrance, CA, USA). The mobile phase consisted of water: methanol:acetonitrile:propionic acid (88:4:8:0.1), the flow rate was 1 ml min^{-1} and the temperature was set at 35 °C. The quantification was performed with the external calibration using standards from Sigma-Aldrich (St. Louis, MO, USA). The S:G:H ratio in lignin was calculated by the following formula: S:G:H = (syringaldehyde + syringic acid) : (vanillin + vanillic acid) : (*p*-hydroxybenzaldehyde + *p*-hydroxybenzoic acid).

2.9 Total RNA isolation

RNA isolation was developed according to Cárdenas-Pérez et al., (2022). Stems of *S. europaea* plants (3 replicates per treatment) were washed with MiliQ water free of RNAse and frozen in liquid nitrogen, and plant material was stored at -80 °C. Total RNA isolation was performed using RNeasy Plant Mini Kit

(Qiagen, Hilden, Germany) following the manufacturer's protocol. RNA's quantity was verified on 1.5% agarose gels in TAE (Tris–HCl, acetic acid, EDTA, pH 8.3) stained with ethidium bromide, and through spectrophotometric measurement (NanoDrop Lite, Thermo Fisher Scientific, Waltham, MA, USA).

2.9.1 Reverse transcription reaction and quantitative real-time PCR (RTqPCR) - *SeNHX1* and *SeSOS1* expression analysis

Before the reverse transcription reaction, the RNA was treated with DNaseI (Thermo Fisher Scientific, Waltham, MA, US). According to the manufacturer's protocol, from 1.5 µg of total RNA using a mixture of 0.25 µg oligo$(dT)_{20}$ primer and 0.2 µg of random hexamers with NG dART RT Kit (Eurx, Gdańsk, Poland), the cDNA was synthesised. The reaction was performed at 25 °C, 10 min, followed by 50 °C, 50 min. The cDNA was stored at -20 °C. The qPCR reaction was performed according to Cárdenas-Pérez et al., (2022); further details are available in the Supporting Information (SI).

2.10 Statistical and multivariate analysis

To evaluate the effect at different concentrations of NaCl in *S. europaea* plants, the relative distances between the different treatments were evaluated using the methodology previously reported by Cárdenas-Pérez et al. and Jaubert-Garibay et al. (Cárdenas-Pérez et al., 2020; Jaubert-Garibay et al., 2022)**.** A principal component analysis (PCA) was developed using XLSTAT software version 2021.4.165. For this analysis, 17 variables were used, (A, mD, AR, R, *E*, Xy diameter, Xy cell wall thickness, Syringic acid, Syringaldehyde, Vanillic acid, Vanillin, *p*-Hydroxybenzoic acid, *p*-Hydroxybenz-aldehyde, Syringyl unit (S), p-Hydroxyphenyl unit (H), *SeSOS1*, *SeNHX1*) arranged in a matrix with the average values obtained from replicates of each treatment and population. A one-way ANOVA comparing treatments was conducted for all the results with the Holm–Sidak method. The relationships between variables were analysed according to Cárdenas-Pérez et al., (2022) further details are available in the SI.

3. Results and discussions

3.1 Changes in salinity modify the structural architecture of Salicornia stems

The thickness of palisade tissue, water-storing parenchyma, and pith regions, which correspond to the AFM-nanoindentation sections analysed at the most representative treatments 0, 400 and 1000 mM NaCl and named “edge”, “middle” and “centre” respectively, were measured. It was detected that salinity induced thickening of middle and centre regions, which also increases along with salinity gradient; in both cases, significant differences were found at 400 and 1000 mM NaCl treatments relative to 0 mM NaCl. By contrast, the edge region showed no significate difference between treatments (Fig. 2).

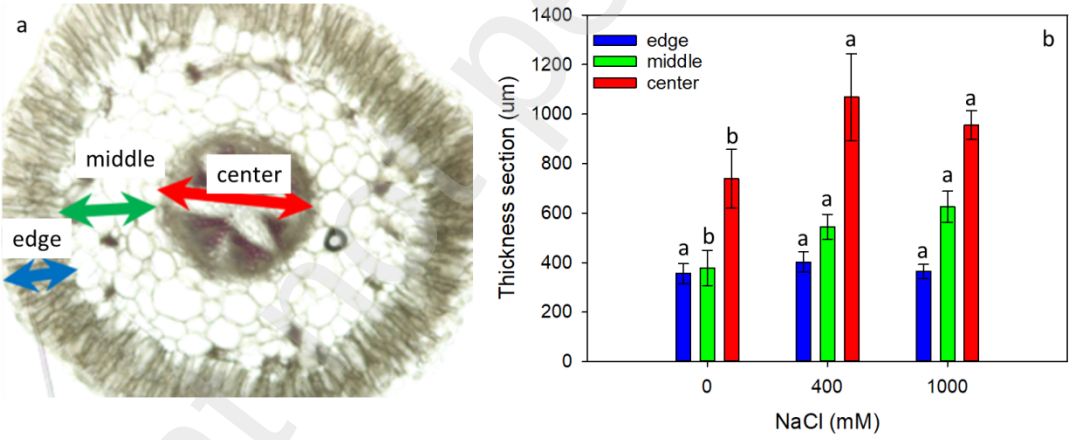

Figure 2. *S. europaea* stem indicating the edge, middle and centre regions (a). Thickness values of the 3 cross regions under 3 treatments (0, 400 and 1000 Mm NaCl) (b). Data represent mean ± SD; different letters indicate significant differences between treatments in each region ($p<0.05$) (n=12).

3.2 Cellular morphometry analysis

An overall observation by light microscopy of the cross-section of *S. europaea* stems showed that the most important changes in cell architecture occurred in the storage parenchyma tissue. Therefore, image analysis (IA) was used to obtain some morphometric parameters from water-storing parenchyma of *S. europaea* (Fig. 3a). Thus, the water-storing parenchyma cells' area (A), major diameter (mD), aspect ratio (AR) and roundness (R) (Fig. 3a) were measured to demonstrate that the cells' size and shape were affected by salinity. A notable increase in A is visible through 200 to 1000 mM of NaCl (Fig. 3 b–f, Table 1). For instance, the percentage increase in A of plants under 400 and 1000 mM was 163% and 246.3% which means that the plants under 400 and 1000 mM swelled 3.5 and 5.4 times the increase in control plants without salinity. This increase was quantified based upon the area rise being converted to a volume, assuming the cell to be spherical. Moreover, the cells under 0 mM treatment have the lowest mD (Fig. 3b), and the highest mD found was at 1000 mM NaCl (Fig. 3f), as expected, while 400 and 600 mM treatments showed no significant differences in mD values (Table 1). The turgidity of the cells was also reflected in the AR and R parameters. The higher the turgidity, the rounder the cells. Additionally, the AR parameter values decrease gradually from 0 to 1000, where 600 and 1000 mM showed significant differences between the rest of the treatments, being lowest at 1000 mM. Then, the R parameter maximum value was found at 1000 mM (Table 1).

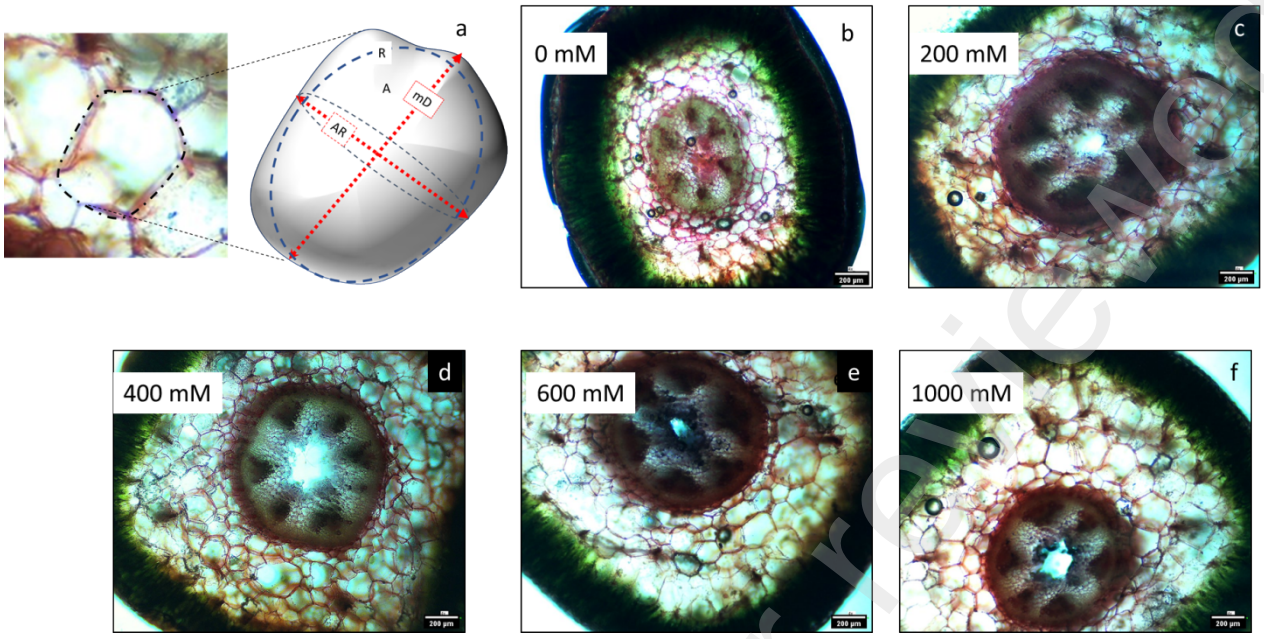

Figure 3. Example of cell image analysis to evaluate morphological parameters (a). *S. europaea* cross-section stem showing changes in cell area under different NaCl treatments (b–f). Scale bar: 200 µm. n=300±50 cells (n=12)

Table 1. Morphometric parameters of *S. europaea* cells under different salinity treatments (n=300)

NaCl (mM)	Area (µm²)	Major diameter (µm)	Aspect Ratio (-)	Roundness (-)
0	6,621.75 ± 340.84^{d}	115.54 ± 3.32^{d}	1.49 ± 0.05^{a}	0.69 ± 0.01^{c}
200	14,270.35 ± 440.35^{c}	164.20 ± 2.58^{c}	1.37 ± 0.02^{bc}	0.75 ± 0.009^{bc}
400	17,347.93 ± 560.54^{b}	176.13 ± 1.88^{b}	1.40 ± 0.02^{ab}	0.74 ± 0.009^{bc}
600	19,649.32 ± 380.53^{ab}	181.68 ± 2.94^{b}	1.33 ± 0.01^{c}	0.76 ± 0.006^{b}
1000	22,771.69 ± 820.26^{a}	202.76 ± 3.47^{a}	1.28 ± 0.01^{d}	0.79 ± 0.007^{a}

Values (mean ± SD) in the same column with different letters are significantly different ($p < 0.05$)

3.3 AFM stiffness distribution of *S. europaea* cells and its correlation with cellular morphometry

To illustrate the overall behaviour of the stem stiffness in each salt treatment, Young's modulus (E) obtained values were organised as frequency histograms, taking into account all values of E along the cross-section of the stem from edge to centre (Fig. 4). The histograms show a wider distribution for 0 and 200 mM with values that ranged from 0.25 MPa up to 4.75 MPa and from 0.20 up to 2.73 MPa, respectively. Then, under the maximum salinity (1000 mM NaCl), the obtained values range from 0.02 MPa up to 0.34 MPa, as shown in Fig. 4. The histograms were properly fitted with an exponential decay function ($y = ae^{-bx}$) and the fit equations are included on the plots and yielded values of R^2 up to 0.99 in all cases. The values "b" of the equations characterise the decay rate of E values. Thus "b" values decrease gradually with the salinity gradient.

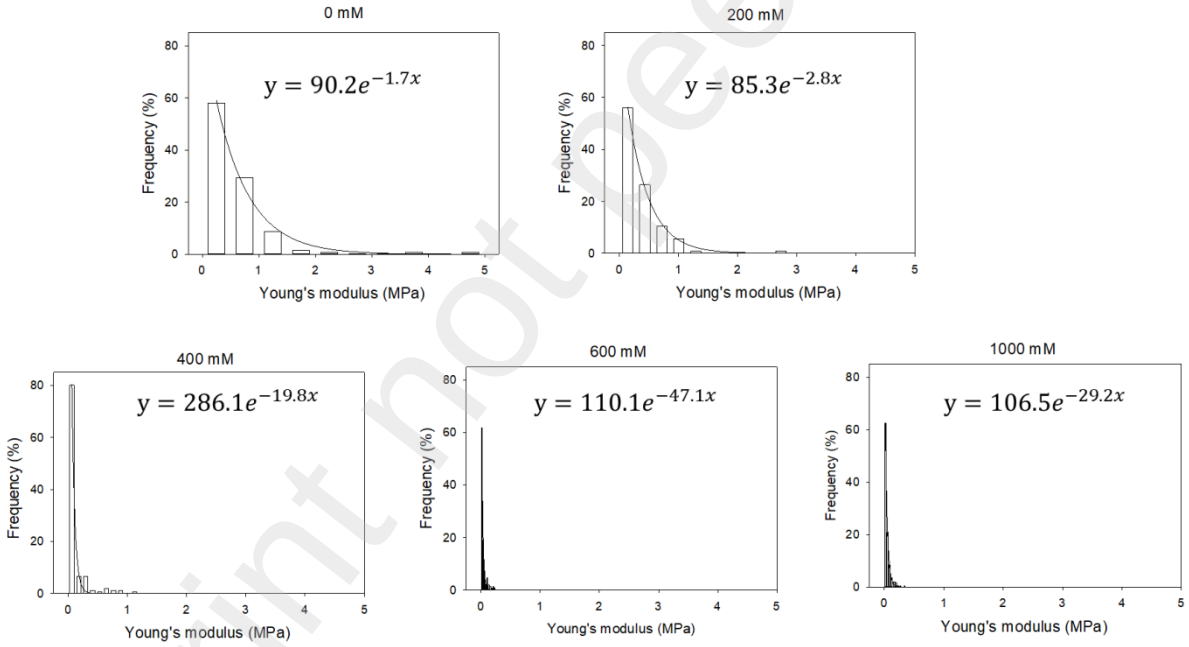

Figure 4. Frequency histograms of Young's modulus values studied at different salinities of *Salicornia* stem cross-sections with their respective fitting curves (+/-1000 force curves, n=3)

To analyse the local stiffness for each cross-section region (edge, middle and centre, see Fig. 5a inset) of the *Salicornia* stems, E values were plotted for each zone. Significant differences were observed in the E

values of the *Salicornia* centre region from 0 to 400 mM in comparison to the other two tested regions (edge and middle).

Then, the *E* values from three cellular surface regions were averaged to visualise stiffness variability in the whole stem. The results indicate an important reduction in *E* along with the salinity gradient from a maximum of 0.53 ±0.05 MPa at 0 mM down to 0.03 ±0.002 MPa at 1000 mM NaCl (Fig. 5b). The reduction in *E* values was also proportional to a higher cell area, allowing water accumulation.

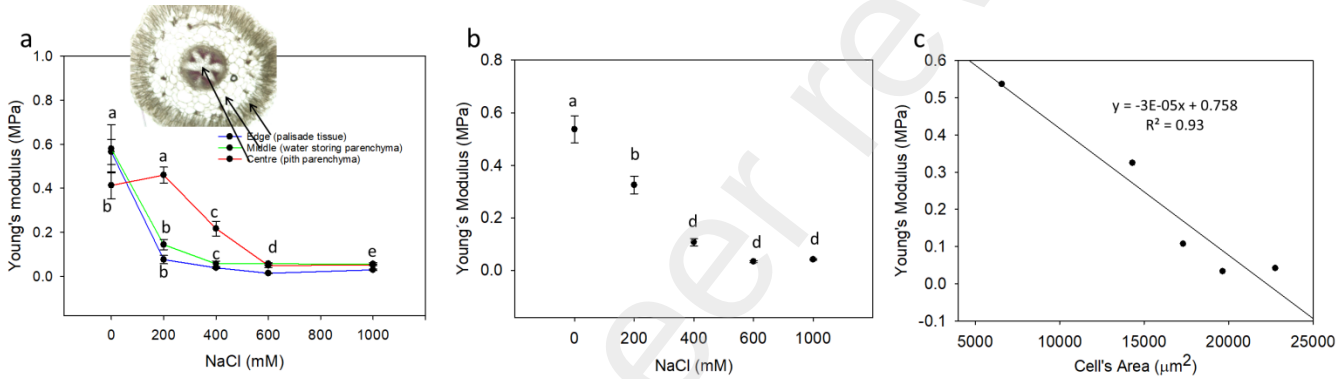

Figure 5. Young's modulus (*E*) values from each stem cross-section region (edge, middle and centre) (a), and averaged *E* values of the whole stem at different salinity treatments from 0 to 1000 mM NaCl (b). Young's modulus correlation *vs* cell's area through the salinity gradient (c). Values obtained are presented as mean values ± standard error. Different letters indicate significant differences between treatments ($p<0.05$), (+/-1000 force curves, n=3)

A proper linear correlation between *E* and cell's area was found with $R^2 = 0.93$ (Fig. 5c). Therefore, in the present *Salicornia* sample, CWE increases along with the increase in cell area through the salinity gradient. This finding settles the remodelling effect in the cell structure through mechanical properties, which, under salt stress, helps to regulate the cell wall elongation.

3.4 Xylem tissue anatomy

The xylem vessel diameter and thickness of lignified xylem cell walls in the stem of *S. europaea* were qualitatively assessed through image analysis in treatments of 0, 400 and 1000 mM NaCl. Both measured parameters increased along with the salinity gradient. In the samples analysed, a substantial increase in xylem diameter and thickness of lignified cell walls was observed at higher salt levels, as shown in Fig. 6a–b.

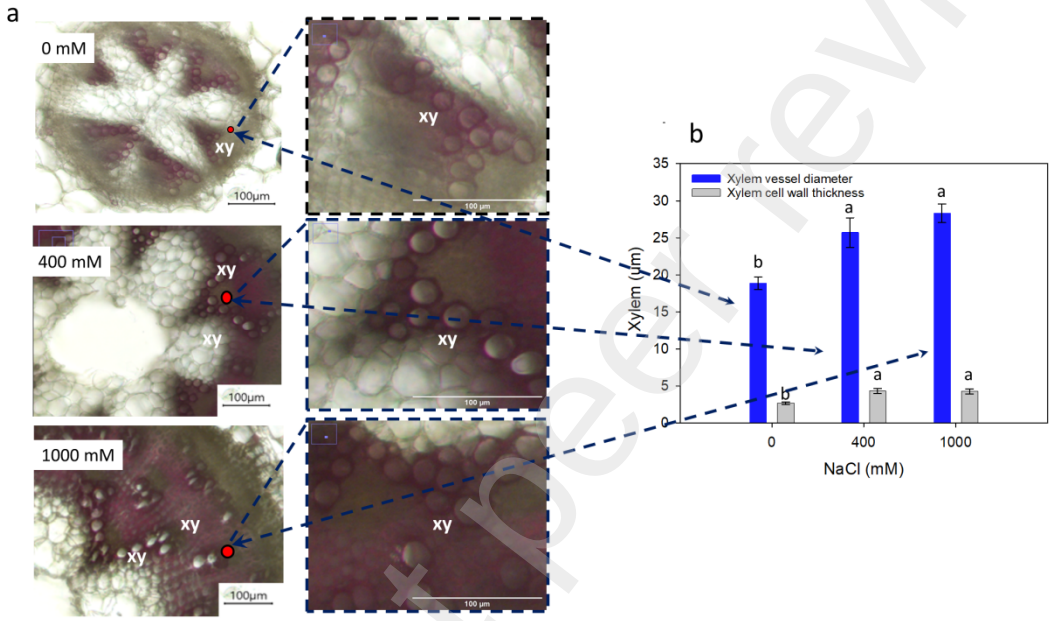

Figure 6. *Salicornia* cross-sections stained with phloroglucinol, lignin is marked red. Xylem vessel diameter and cell wall thickness under 3 treatments 0, 400 and 1000 mM NaCl. Light microscopy images showing the evaluated xylem vessels. Scale bar 100 µm (a). Xylem vessel diameter and cell wall thickness values plotted (b). Data represent mean ±SD, different letters indicate significant differences between treatments ($p<0.05$) (n=12)

Salicornia vessels located out of the stele, in the cortical tissues, were also analysed for the same treatments (0, 400 and 1000 mM NaCl). They showed the same proportional increase in diameter and cell wall thickness as shown in Fig. 7 a', c' and e'. A substantial growth in the number of vessels and a visible difference in central stele architecture were also found for higher salt levels. For instance, Fig. 7b shows

inside the pericycle, five vascular bundles in circular arrangement for plants under 0 mM treatment, while for plants under 400 and 1000 mM, six and seven vascular bundles are present, respectively (Fig. 7 d, f).

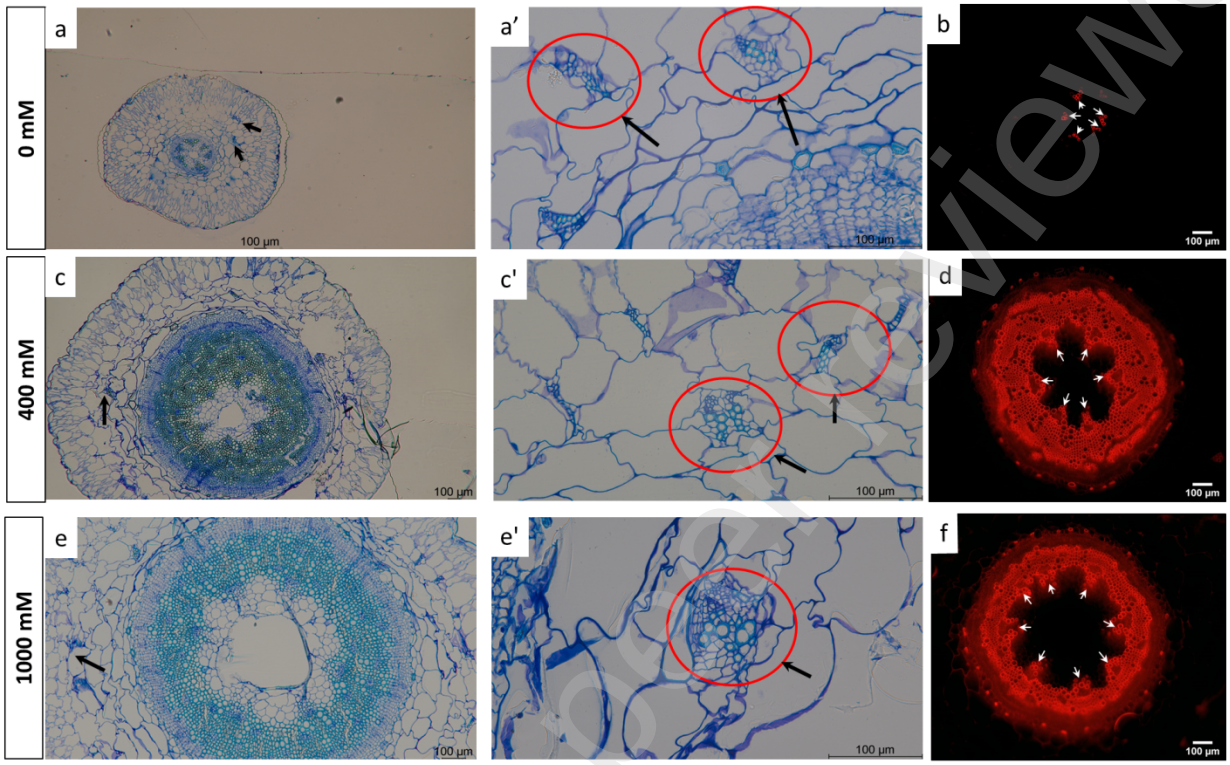

Figure 7. *Salicornia* stem cross-sections stained with toluidine blue (a,c,e) and basic fuchsin (b,d,f), showing lignin in green-blue and red, respectively. Light microscopy images showing xylem vessels at a. 0, c. 400 and e. 1000 mM NaCl. Note xylem vessels located out of the stele in the cortical tissue (arrow) in the magnified view of the xylem vessels out of the stele for the same treatments (a'c'e'). Vascular bundles inside the stele for the same treatments (arrows) (b.d.f). Scale bar: 100 µm, (n=12)

3.5 Lignin monomer composition

Nitrobenzene oxidation (NBO) analysis revealed that samples receiving no NaCl treatment differed substantially in their lignin monomer composition (Table 2). Plant stems were rich in syringyl (S) units, whereas the total proportion of both guaiacyl (G) and *p*-hydroxyphenyl (H) units was lower than that of S units. The increased concentrations of NaCl caused a drop in the proportion of S units. At the treatment of

1000 mM NaCl, lignin in stems might be more condensed in both G and H than in S units, which became the prevailing monomers in the macromolecule. Interestingly, the highest proportion of H units was found in the plant stems receiving 1000 mM NaCl.

Table 2. Yields of nitrobenzene oxidation products (% of oven-dry extracted biomass). Values (mean ±SD) in the same column with different letters are significantly different ($p < 0.05$) (n=3).

Treatment (mM NaCl)	Syringic acid	Syringaldehyde	Vanillic acid	Vanillin	*p*-Hydroxybenzoic acid	*p*-Hydroxybenz-aldehyde	Total yield	S : G : H ratio
0	0.26 ± 0.01 ^{b}	0.37 ± 0.00 ^{b}	0.11 ± 0.00 ^{b}	0.19 ± 0.01 ^{b}	0.03 ± 0.00 ^{d}	0.11 ± 0.00 ^{b}	1.07 ± 0.01 ^{b}	2.06 : 1 : 0.46
200	0.25 ± 0.02 ^{bc}	0.25 ± 0.01 ^{d}	0.12 ± 0.02 ^{b}	0.15 ± 0.01 ^{c}	0.03 ± 0.00 ^{d}	0.09 ± 0.01 ^{b}	0.89 ± 0.02 ^{b}	1.83 : 1 : 0.45
400	0.33 ± 0.04 ^{a}	0.76 ± 0.13 ^{a}	0.14 ± 0.02 ^{b}	0.29 ± 0.03 ^{a}	0.06 ± 0.01 ^{bc}	0.15 ± 0.01 ^{a}	1.84 ± 0.36 ^{a}	2.39 : 1 : 0.48
600	0.26 ± 0.02 ^{b}	0.34 ± 0.04 ^{bc}	0.18 ± 0.04 ^{a}	0.17 ± 0.02 ^{bc}	0.07 ± 0.01 ^{b}	0.16 ± 0.02 ^{a}	1.05 ± 0.15 ^{b}	1.58 : 1 : 0.60
1000	0.32 ± 0.02 ^{a}	0.13 ± 0.00 ^{e}	0.19 ± 0.02 ^{a}	0.08 ± 0.00 ^{d}	0.13 ± 0.03 ^{a}	0.17 ± 0.02 ^{a}	1.08 ± 0.10 ^{b}	1.65 : 1 : 1.29

An important measure of lignin composition in plant cell walls is the ratio of S, G and H units. The most abundant S and G units interact together to form the polymer's backbone via a labile arylglycerol-β-aryl ether (β-*O*-4) bond (Santos et al., 2012). Lignins rich in both G and H units are prone to condensation reactions. Lignin rich in G units has relatively more carbon–carbon bonds than lignin rich in S units because the aromatic C-5 ring position of G units is free to make linkages. A high S/G ratio may lead to larger linear chains, and such a lignin type presents a more open matrix (Lourenço et al., 2015). In addition, a positive correlation between S/G ratio and sugar yields is associated with bioethanol production, as reported in fast-growing natural poplars (Dumitrache et al., 2016; Yoo et al., 2018). Therefore, plant-breeding strategies in the bioenergy industry are trying to select plants with high S/G ratios (Bose et al., 2009; Ďurkovič et al., 2020). In this study, high S/G ratios were found just for the treatments 0–400 mM NaCl. On the other hand, a high salinity stress negatively affected the proportion of S units but increased H units (Table 2). H-rich lignin is more condensed than S-rich lignin, and therefore energetically more stable (more C–C bonds) against depolymerisation.

3.6 SEM-EDX observations

S. europaea stems were scanned via SEM-X-ray microanalysis from the water parenchyma cells (Fig. 8). It was detected that plants under 0 mM treatment (Fig. 8a) have small oxalate crystals as compared to the large oxalate crystals found under 1000 NaCl treatment (Fig. 8c). The calcium oxalate crystals finding was confirmed in the elemental composition of the water parenchyma cells (Fig. 8b and d).

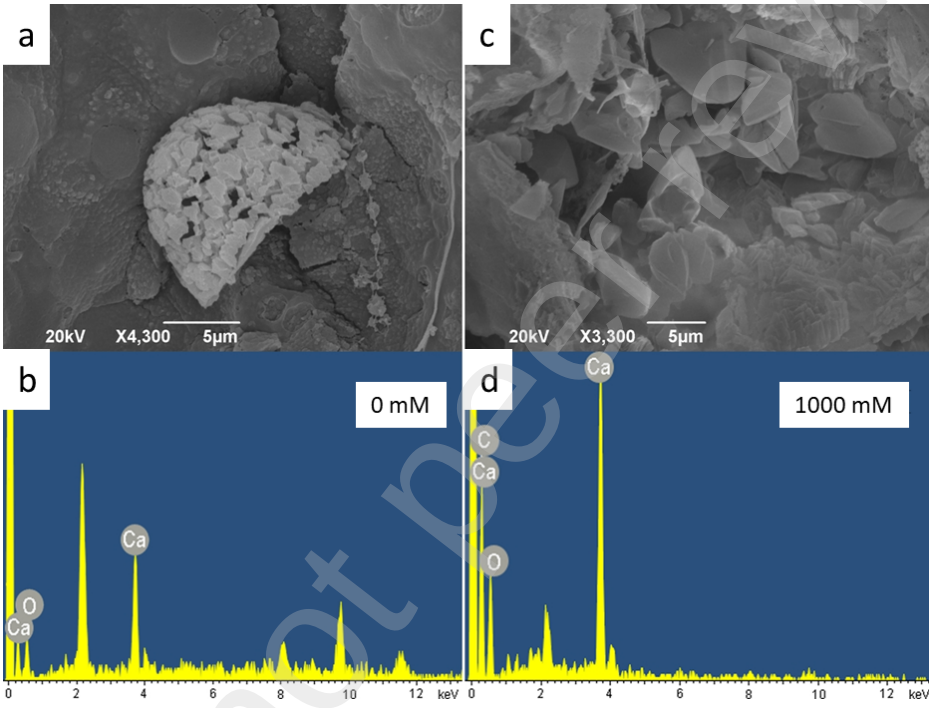

Figure 8. Scanning electron microscopy images of oxalate crystals deposited in the *S. europaea* stem tissue. Calcium oxalate druse in the cortex parenchyma cell with its EDX spectra at 0 mM (a,b) and 1000 mM NaCl treatment (c,d). Scale bar 5 µm (n=3)

The presence of both Na and Cl peaks in cell walls and lumens of cortex cells was also confirmed for the 400 and 1000 NaCl treatments, and the absence of them at 0 mM, by SEM-EDX analysis (Fig. 9).

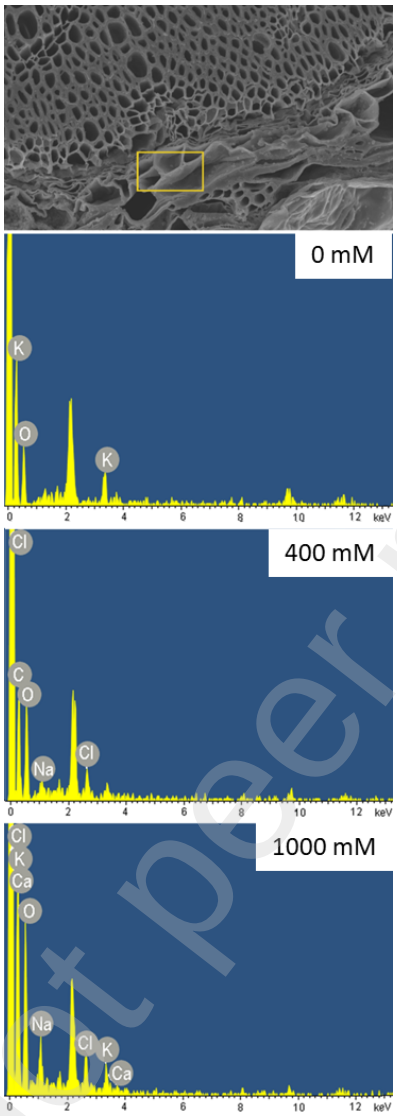

496

497 **Figure 9.** Representative scanning electron microscopy image of the *S. europaea* stem cross-section
498 (upper image) showing the cortex region (yellow rectangle) in which the EDX spectra were obtained for
499 the assessment of the elemental composition at 0, 400 and 1000 mM NaCl, (n=3)

500 **3.7 *S. europaea* expression patterns of *SeSOS1* and *SeNHX1* genes involved in Na^+ exclusion**

501 The expression of *S. europaea* genes *NHX1* and *SOS1* at different saline treatments was analysed using
502 quantitative reverse transcriptase polymerase chain reaction (RT-qPCR). The analysed *NHX1* and *SOS1*
503 genes encode a tonoplast Na^+/H^+ antiporter and an apoplast Na^+/H^+ antiporter, respectively. Mainly
504 *SeNHX1* shows significant upregulation in plants grown in saline conditions at 200, 400, 600 and 1000

mM NaCl compared to non-saline treatment, while *SeSOS1* expression increased only in plants at 200 and 400 mM NaCl in comparison to the non-saline treatment (Fig. 10).

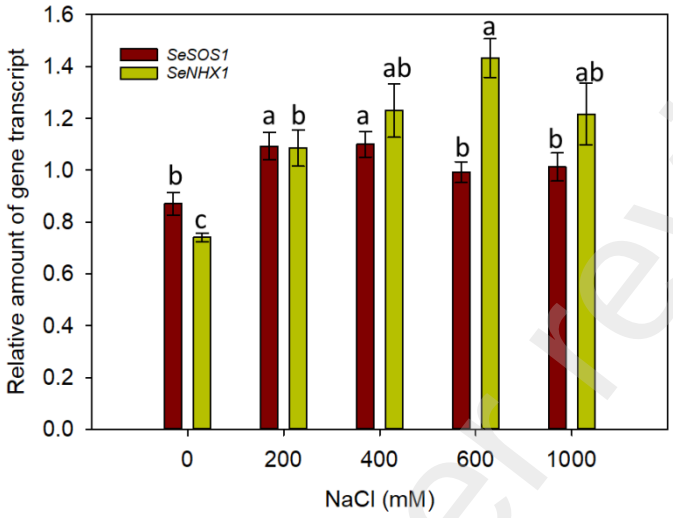

Figure 10. Expression pattern of *SeNHX1* and *SeSOS1* genes involved in stems of *S. europaea* sodium segregation under different NaCl concentrations. Means ± standard error of replicates. Different letters indicate significant differences between treatments ($p < 0.05$) (n=3)

3.8 *S. europaea* data multivariate analysis

For a better visualisation of the correlations between the studied variables, a principal component analysis (PCA) was performed to investigate the multidimensional datasets with the quantitative variables. Figure 11a shows the PC1 and PC2 axes, which accurately describe the variance of the samples (85.9%). This plot shows how studied variables of the plant, behave with regard to saline stress and how they move through the two-dimensional space of the main components, from the negative quadrant of PC1 to the positive quadrant of PC1 as long as salinity increases. The results were also grouped on a 3D plot (Fig. 11b) according to their similarities through the three principal factor scores (PC1, PC2 and PC3), which describe the variability of the samples (95%). Figure 11c aims to highlight the dynamic modifications of the cell wall in terms of elasticity, which is pretty correlated with all the studied variables.

To evaluate the behaviour of all the variables between treatments, we plotted the three main principal components represented in 3D. Figure 11b shows the corresponding distances, considering 0, the point of comparison between 200, 400, 600, and 1000, representing the modifications driven by the saline concentrations in mM.

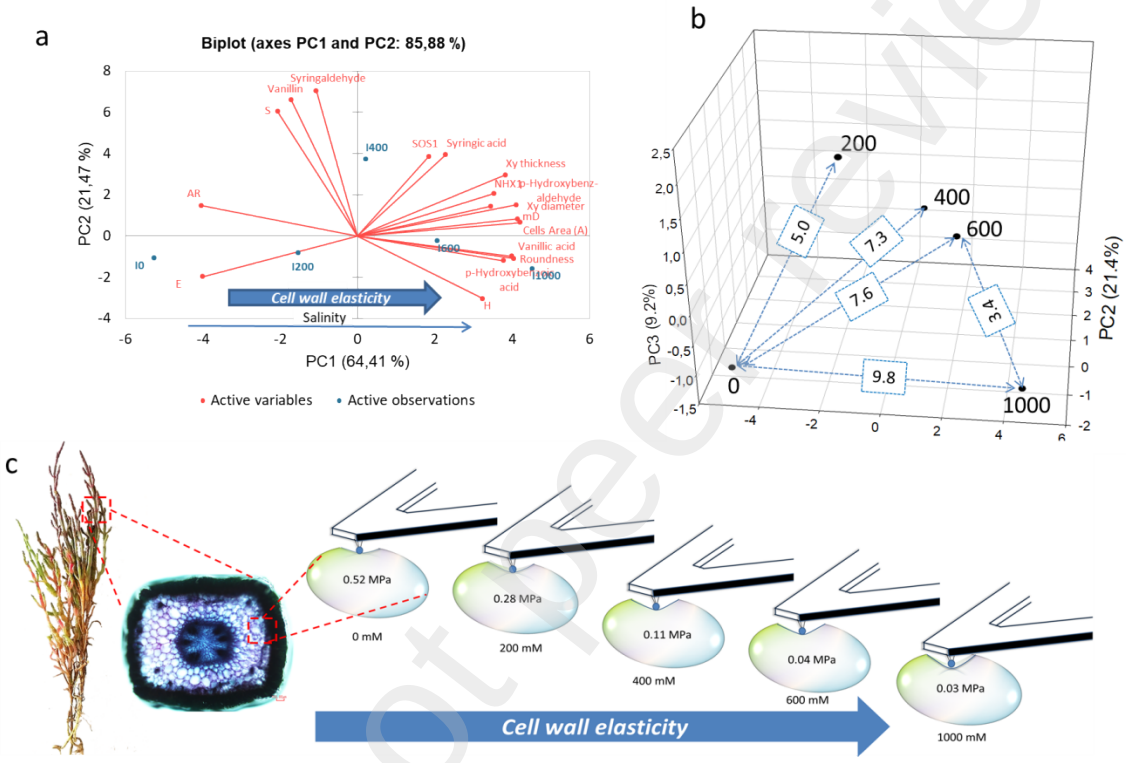

Figure 11. Bi-plot of the first two principal components with all variables and observations, showing the distribution of samples along the gradient of salinity from right to left I0 to I1000 mM (a). Three main principal components are represented in a 3D plot with their corresponding distances, considering 0 the point of comparison between 200, 400, 600, and 1000 mM NaCl (b). A depicted representation of the cell wall elasticity driven by salinity through AFM analysis(c). A: cell's area, *E*: Young's modulus, S: S lignin unit, H: H lignin unit, mD: cell's major diameter , AR: cell's aspect ratio, R: cell's roundness

4. Discussion

The image analysis used for morphometry stem analysis showed that the greater water-storing parenchyma and diameter pith of *S. europaea* was at high salinities, 400 and 1000 mM (Fig. 2). This could be due to the increase in the water-storing cells' size and turgidity, which is stimulated by salinity in *S. europaea*. As reported in previous studies (Cárdenas-Pérez et al., 2022; Debez et al., 2006; Grigore and Toma, 2020), the increase in stem water-storing parenchyma succulence allows a higher vacuole volume, and this may increase the capacity for storing ions, which may translate into better adaptation to saline environments.

The morphometric changes also showed that cells' roundness increased along with salinity. For instance, at 1000 mM, AR showed the lowest values. These findings could be due to a decrease in the mechanical strength of the cell wall caused by the cell's water accumulation, promoting a cellular rearrangement and architecture-structure loss of the cells in the tissue. Therefore, it is possible to assume that salinity stress in this species induces the cells to expand and cell walls to lose rigidity, making them rounder. This result may explain why *S. europaea* water-storing parenchyma cells seemed bigger at higher salinities.

The AFM results plotted in histograms exhibited the cell wall stiffness (*E*) drop from 0 to 1000 NaCl as an important finding. This result may indicate a higher and homogeneous CWE associated with the cells' elongation due to higher turgidity. This trait can be attributed to a physiological mechanism of the plant's cells to cope with salinity. Some authors consider CWE an essential way of adaptation to water stress (Hessini et al., 2009; Martínez et al., 2007; Patakas et al., 2002). For instance, these authors tested the CWE through indirect measurements by evaluating the effect of water stress on the osmotic cell wall and cell volume of *Spartina alterniflora* Loisel and in cultivar beans. They observed that the elasticity in the cell wall is an important mechanism that helps preserve proper cell volume and turgor. Many authors have reported that the increase in CWE can promote a better cell volume and turgidity when the plant is subjected to some water stress; this is the case for wheat, grapevine, common beans and olive tree, among others (Colin et al., 2023; Dichio et al., 2003; Hessini et al., 2009; Martínez et al., 2007; Patakas et al., 2002).

Our results agree with Martínez et al., (2007), who reported that when three tested common bean cultivars (Orfeo, Tortola and Pinto) with high salt tolerance are subjected to drought, they experiment with a substantial increase in CWE (or low elastic modulus). Those authors associated this attribute with an essential physiological adjustment role in the cell wall that helps to maintain the plant's cell turgidity better, this was also stated by Rui and Dinneny, (2020). In contrast, another tested cultivar, Arroz Tuscola, considered salt sensitive, did not present higher cell wall elasticity. While very few studies have tested CWE in halophytes, Liu et al., (2022) tested mechanical parameters using a creep-meter equipment (less sensitive than AFM). They reported that salinity significantly reduced CWE in *S. oleracea* roots, whereas treatment with up to 200 mM NaCl increased it in *S. salsa*, a more salt-resistant halophyte. They suggested that the high content of lignin-cellulose and pectin in the cell wall induced the elasticity and may be a salt tolerance mechanism that protects the cell structure's stability under salt stress in halophytes compared to glycophytes.

Additionally, in the centre region of the stem, it was found that *E* values did not change significantly from 0 to 200 and, this region maintained higher rigidity at 400 mM compared to the edge and middle regions (Fig. 5a). This can be attributed to the presence of lignified cells, parenchyma cells or sclerenchyma cells that lie just inside the endodermis, because the centre or pith region in *Salicornia* is a more-or-less cylindrical body of tissue in the centre of the axis, enclosed by vascular and parenchymatic tissues in which the cells are arranged usually loosely. Therefore, the tested stiffness in the centre region is expected to be more heterogeneous and stiffer than the other regions. In edge and middle regions, a remarkable decrease is detected from non-saline to 200 and 400 mM, but at 600 and 1000 mM the stiffness drops substantially for all regions.

Results from Zörb et al., (2015) are similar to our findings. They used a linear variable differential transducer to test cell wall elasticity indirectly, which is less precise than AFM. They found that, under salt stress, the salt-tolerant maise epidermal cell walls were more extensible. This elasticity allowed cell

turgidity and leaf growth to be maintained under salinity, whereas the sensitive maise exhibited noticeably stiffer epidermal cell walls linked to leaf growth reduction under stress.

In the present study, AFM allows us to measure directly the CWE in-vivo. It increases along with the increase in cell area through the salinity gradient. This finding settles the remodelling effect in the cell structure through mechanical properties, which, under salt stress, help to regulate cell wall elongation. The morphometric characterisation of cells through image analysis was an essential tool. For instance, in future studies, it could be possible to infer at first sight what changes are occurring inside the cells based on their mechanical properties.

Moreover, Cárdenas-Pérez et al., (2022) already reported that, under salt stress, highly salt-tolerant plants such as *Salicornia* species have cells with high levels of methyl-esterified pectin. It allows a denser and more extensible cell wall and promotes the swelling of the cells.

The increase in xylem diameter, along with salinity gradient, indicates that the plant is efficiently using the xylem vessels' water transport to cope with salinity. Because xylem vessel diameter and thickness parameters were shown to be higher at (400 and 1000 mM) than at 0 mM (Fig. 6b).

Our results also suggest that salinity enhances structural changes in the stem of *S. europaea*. The diameter of xylem cells, their abundance and xylem cell wall thickness increased with the rise in saline concentration (Fig. 6 and 7 a', b, c', d and e', f). Sánchez-Aguayo et al., (2004) reported that salt stress enhances xylem development in lignifying tissues of tomato plants grown under salinity. For instance, they found statistical differences between the average sizes of the areas occupied by lignified cells in control and salt-treated tomato plants. This difference constituted a two-fold increase in lignified cell number in stem plants subjected to salinity compared to a non-saline control. Their results indicate that salinity enhanced the development and abundance of lignified cells' vascular bundles. The gain in the enhanced cell wall lignification may be a straightforward structural adaptation of plants to salinity that improves water flow through the plant. The vessels' number and diameter are essential factors for both

effective water transport through the plant and mechanical support when coping to salt stress (Grigore and Toma, 2020; Sánchez-Aguayo et al., 2004; Schreiber et al., 2015).

The lignin composition also plays an essential role in plant salt tolerance. Lignin rich in G units has relatively more carbon–carbon bonds than lignin rich in S units. A high S/G ratio may lead to larger linear chains, and such a lignin type presents a more open matrix (Lourenço et al., 2015). In addition, a positive correlation between S/G ratio and sugar yields is associated with bioethanol production, as reported in fast-growing natural poplars (Dumitrache et al., 2016; Yoo et al., 2018). Therefore, plant-breeding strategies in sustainable remediation try to select plants with high S/G ratios (Bose et al., 2009; Ďurkovič et al., 2020). In this study, high S/G ratios were found just for the treatments 0–400 mM NaCl. On the other hand, a high salinity stress negatively affected the proportion of S units but increased H units (Table 2). According to Hori et al., Le Gall et al. and Tenhaken (Hori et al., 2020; Le Gall et al., 2015; Tenhaken, 2015), decreasing the lignin S/G ratio may change the rigidity and hydrophobicity of the cell walls. So, they proposed that the lower S/G ratio could be a scheme of some species to increase their cells' hydrophobicity when subjected to salt stress and/or drought. For instance, it has been reported that the reduced S/G in vessels is related to the activity of water transportation (Abreu et al., 2009; Li et al., 2001; Saito et al., 2012).

The large calcium oxalate crystals found through SEM in this study at high salinity, confirm the evidence reported in previous studies (Franceschi and Horner, 2014; Franceschi and Nakata, 2005) that the synthesis of calcium oxalate and its abundance, besides its already known function as structural supports. The bunch of oxalate crystals thus may be a manifestation of an effort to maintain ionic equilibrium. Interestingly, Tooulakou et al., (2016) stated that when the entry of atmospheric CO_2 is limited in plants due to the closing of stomata, such as under drought or high-salinity conditions. They provided evidence that calcium oxalate crystals represent active pools of carbon that can supply CO_2 to photosynthetic cells when stomata are fairly or closed.

Lv et al., (2012) demonstrated that when *S. europaea* is subjected to salt stress, Na^+ is compartmentalised predominantly into the endodermis tissues, whereas, at the subcellular level, Na^+ is compartmentalised into the cell vacuoles. Our results agree with those reported by Lu et al., (2003), where *Suaeda salsa* L. Pall. has the ability to take up and confine Na^+ to stems, through a mechanism that aids water uptake and transport. The spatial distribution of inorganic crystals across the stem tissues at 1000 mM NaCl treatment may be seen in the Supplementary Material Videos S1 and S2.

Here we also demonstrated that the Na^+ tolerance phenomenon in the plant is overcome by sequestering the excess of Na^+ into the vacuole, which prevents toxic levels of Na^+ accumulation in the cytoplasm. According to Lv et al., (2012), one of the Na^+/H^+ antiporters in the tonoplast responsible for Na^+ transport from cytosol to the vacuole is *NHX1*, which plays a central role in salinity tolerance and cell wall remodelling. This role is identified by many authors as vacuolar Na^+ sequestration (Barragán et al., 2012; Munns and Tester, 2008; Solis et al., 2022) and is considered to be a key trait in non-sensitive salt crops and halophytes, including *S. europaea* (Lv et al., 2012; Solis et al., 2022; Yang et al., 2011).

In the present study, *SeNHX1* was significantly expressed at high salinity (Fig.10), suggesting the vital role of Na^+/H^+ in the Na^+ influx to the vacuole in plant cells. For instance, Hayatsu et al., (2014) reported that, in the halophyte *Sonneratia alba* Sm., the Na^+ content in the vacuole was higher than in glycophyte *Oryza sativa* L. Therefore, the Na^+ vacuolar sequestration helps to promote cell turgor pressure maintenance in the plant by allowing cells in the stem to expand during growth development under high-salinity conditions. Jha et al., (2011) stated that the *SbNHX1* gene was also highly expressed for *Salicornia brachiata* Roxb. under high NaCl concentrations.

Fig.11a graphically shows how the studied active variables are described through the plant's low and high salt gradient, as well as how *S. europaea* plants undergo physiological changes to cope better with salinity. The biplot shows the remarkable correlation between morphometric parameters such as the cell's area and roundness with the low Young's modulus (*E*) values, influenced by salinity, which infer a cell's expansion to promote water accumulation. This correlation is also described numerically in the Pearson correlation in

supplementary Table S1, where *E* has a strong negative correlation with the cell's area (-0.97), xylem diameter (-0.96) and xylem thickness (-0.94). The biplot graphically demonstrates that cell stiffness is inversely proportional to salinity. At the same time, we also show the significant correlation of morphometric parameters such as cell area and roundness to high salinity.

Furthermore, factorial scores in 3D plot (Fig. 11b) consider 0 as the point of comparison between 200, 400, 600, and 1000Mm NaCl. The distances indicate that the greater the stress, the greater the separation from 0. While distances between 200, 400 and 600 are shorter, variables under these treatments behave similarly and may be the optimal range of salinity where this species can grow well. The shortest and highest separation with 0 occurred at 200 mM (distance = 5) and 1000 mM (distance = 9.8), respectively. An image growth analysis reported in a previous salinity tolerance study (Cárdenas-Pérez et al., 2020; Cárdenas-Pérez et al., 2022) agreed with our observed results for the same population – that, under higher salinity, the plant developed better, with higher succulence than at non-saline treatment. *SeNHX1* has a high negative correlation with the *E* (-0.95), indicating that when the plant experiments with a high Na^+ influx to the vacuole, the cell wall rigidity is very low (Table S1). The present results confirm our hypothesis that salinity induced a nano-mechanical and compositional remodelling in cells to facilitate water accumulation for *S. europaea*. To our knowledge, these results, especially the direct cell wall stiffness measurements by AFM, are presented for the first time and set the tone for future studies. Figure 11c highlights the changes in the cell wall elasticity driven by salinity, which can be considered a vital analysis trait when scientists seek for highly resistant plants. Our results give rise to the future study of the nano-mechanical properties of cell walls as a factor influencing the resistance to salinity in halophytes and crop plants.

5. Conclusions

Our results are consistent with the role of physiological adjustments in cell wall elasticity (CWE) as an essential trait in the resistance to salt stress. We confirmed that *S. europaea* uses different structure-function mechanisms to tolerate high salinity. The factors that come into effect under higher salinities to

contribute significantly to maintaining cell turgor (which is essential for normal cell functions under low water activity) are: increased CWE; increased cell size; shape remodelling; well-developed palisade tissue, water-storing parenchyma and pith regions; thickening of xylem vessels diameter and cell walls; and an increased number of vascular bundles. Our results are important as an insight to understand plant adaptation. In future, researchers can gain insights into the structural adaptations by measuring cell wall elasticity that enable these plants to withstand osmotic stress caused by salt. This knowledge can contribute to a better understanding of plant adaptation strategies to extreme environments. Because the cell wall is a dynamic structure that plays a crucial role in plant growth, development, and response to environmental stresses. Measuring cell wall elasticity through AFM allows researchers to quantify the mechanical properties of the cell wall, such as stiffness, flexibility, and viscoelastic behaviour. This information helps in understanding how the cell wall responds to salt stress and how it influences plant growth and survival. Our approach, expose how *Salicornia* plants possess unique mechanisms to cope with high salt concentrations through cell wall elasticity measurements. Future studies can be done to evaluate the impact of salt stress on the mechanical properties of the cell walls of different plants. For example, changes in elasticity can indicate alterations in cell wall composition, organisation, or integrity, providing insights into the plant's salt tolerance mechanisms. We propose future studies for comparing the cell wall elasticity of *Salicornia* with non-halophytic plant species. This can help to identify specific adaptations that contribute to salt tolerance. In this line, AFM measurements can provide quantitative data on how the cell wall properties differ between halophytes and non-halophytes, aiding in the identification of key factors that enable halophytes to thrive in high-salinity conditions. Also, the understanding of the cell wall elasticity in high salt-resistant halophytes can have implications for crop improvement. By identifying the specific cell wall properties that contribute to salt tolerance, researchers can potentially engineer these traits into crop plants, enhancing their ability to withstand saline conditions and improving agricultural productivity in salt-affected regions. In summary, measuring cell wall elasticity in high salt-resistant halophytes is crucial for understanding plant adaptation, unravelling cell wall mechanics,

assessing salt tolerance mechanisms, comparing different plant species, and potentially engineering salt-tolerant crops.

Supplementary Material

Supplementary Figures

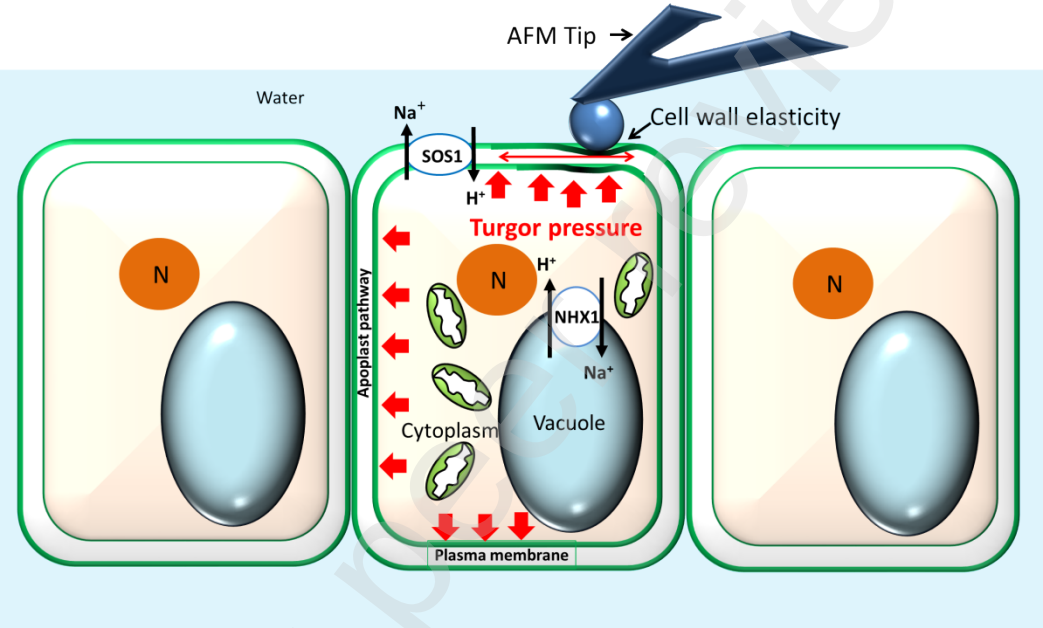

Figure S1. Diagram of *S. europaea* stem tissue indicating the antiporters *NHX1* and *SOS1* located in tonoplasts and apoplast respectively as well as the turgor pressure and cell wall elasticity while performing AFM nanoindentation

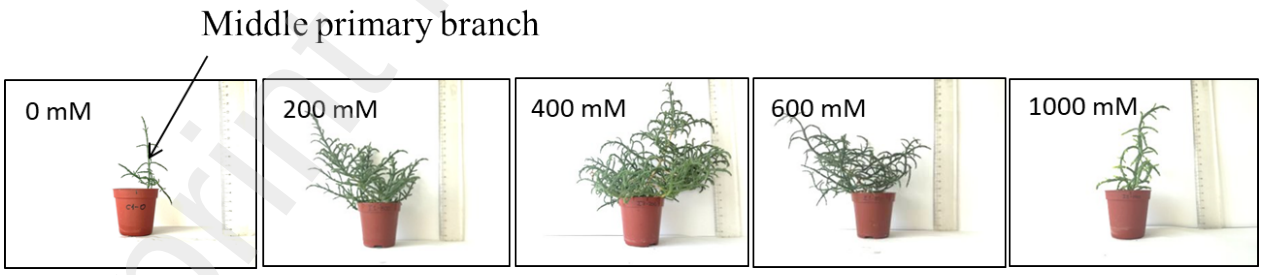

Figure S2. *S. europaea* plant treatments (0, 200, 400, 600, and 1000 mM NaCl) arrow indicates the middle primary branch section from where cross-section samples were obtained

Statistical and multivariate analysis

The relationships between variables were performed using a Pearson analysis, while a significance test (Kaisere–Meyere–Olkin) was performed to determine which variables had a significant correlation with each other (α=0.05). Then, a 3D plot was developed using the three principal component factors according to the Kaiser criterion. The three main factorial scores of the PCA from each sample were used to calculate the distance (D) between the two points under different treatments, P1= (x_1, y_1, z_1) and P2= (x_2, y_2, z_2) present in the 3D space of the PCA. (Eq.3)

$$D(P1,P2) = \sqrt{(x_2 - x_1)^2 + (y_2 - y_1)^2 + (z_2 - z_1)^2} \quad (3)$$

where *x*, *y*, and *z* are the three main factorial scores in the PCA, *P1* corresponds to the non-saline treatment point and *P2* to each of the other salt treatments points 200, 400, 600 and 1000 respectively. Relative distances were used to evaluate and determine in which salt treatments the greatest differences were recorded.

Reverse transcription reaction and quantitative real time PCR (RT-qPCR) - *SeNHX1* and *SeSOS1* expression analysis

The PCR reaction mixture includes 4 µL of 1/20 diluted cDNA, 0.5 µM gene-specific primers (the same as used by Cárdenas-Pérez et al., (2022) and 5 µL of LightCycler 480 SYBR Green I Master (Roche, Penzberg, Germany) in a total volume of 10 µL. Clathrin adaptor complexes was used as a reference gene (Xiao et al., 2015). The reaction was performed in triplicate (technical replicates) in LightCycler 480 Instrument II (Roche, Penzberg, Germany). The thermal cycling conditions were as follows: initial denaturation 95 °C for 5 min, 40 cycles of 95 °C for 10 s, 60 °C for 20 s, 72 °C for 20 s. The SYBR Green I fluorescence signal was recorded at the end of the extension step in each cycle. The specificity of the assay was confirmed by the melt curve analysis i.e., increasing the temperature from 55 °C to 95 °C at a ramp rate 0.11 °C/s. The fold-change in gene expression was calculated using LightCycler 480 Software release 1.5.1.62 (Roche, Penzberg, Germany).

Supplementary Videos

Video S1. X-ray micro-computed tomography longitudinal imaging of the *S. europaea* stem (0 mM NaCl treatment) showing the spatial distribution of inorganic crystals (white dots). Scale bar 0.3 mm

Video S2. X-ray micro-computed tomography longitudinal imaging of the *S. europaea* stem (1000 mM NaCl treatment) showing the spatial distribution of inorganic crystals. Scale bar 0.5 mm

Supplementary Table

Table S1. Pearson correlation matrix of all analysed variables. Values in bold are different from 0 with a significance level α=0.05. A: cell's area, *E*: Young's modulus, S: S lignin unit, H: H lignin unit, mD: cell's major diameter , AR: cell's aspect ratio, R: cell's roundness

Variables	A	*E*	S	H	Xy diam.	Xy thick.	Syringic acid	Syringaldehyde	Vanillic acid	Vanillin	*p*-Hydroxybenzoic acid	*p*-Hydroxybenz-aldehyde (H.b.a.)	*SOS1*	*NHX1*	mD	AR	R
A	**1**																
E	**-0.972**	**1**															
S	-0.428	0.296	**1**														
H	0.682	-0.518	-0.563	**1**													
Xy diameter	**0.962**	**-0.958**	-0.283	0.694	**1**												
Xy thickness	**0.943**	**-0.987**	-0.155	0.442	**0.935**	**1**											
Syringic acid	0.536	-0.530	0.373	0.511	0.678	0.598	**1**										
Syringaldehyde	-0.174	-0.019	**0.911**	-0.570	-0.025	0.148	0.393	**1**									
Vanillic acid	**0.905**	-0.870	-0.583	0.770	**0.923**	0.787	0.416	-0.319	**1**								
Vanillin	-0.325	0.123	**0.911**	-0.713	-0.193	0.002	0.216	**0.982**	-0.456	**1**							
p-H. acid	0.831	-0.730	-0.453	**0.948**	**0.878**	0.669	0.648	-0.347	**0.897**	-0.515	**1**						
p-H.b.a.	0.777	-0.801	-0.186	0.654	**0.911**	0.759	0.670	0.064	**0.890**	-0.094	0.849	**1**					
SOS1	0.541	-0.572	0.162	-0.021	0.416	0.669	0.367	0.282	0.136	0.210	0.107	0.057	**1**				
NHX1	**0.880**	**-0.953**	-0.316	0.288	0.837	**0.935**	0.292	0.059	0.783	-0.039	0.522	0.676	0.569	**1**			
mD	**0.992**	**-0.955**	-0.396	0.661	**0.935**	**0.940**	0.546	-0.166	0.849	-0.316	0.799	0.708	0.626	0.858	**1**		
AR	**-0.949**	0.867	0.666	-0.737	-0.846	-0.808	-0.317	0.461	-0.876	0.582	-0.802	-0.620	-0.465	-0.790	**-0.948**	**1**	
R	**0.953**	-0.869	-0.608	0.732	0.848	0.824	0.372	-0.420	0.843	-0.548	0.798	0.599	0.534	0.778	**0.963**	**-0.995**	**1**

Conflicts of interest

There are no conflicts to declare.

Acknowledgement

This work was created due to the research project No. 2021/43/D/NZ8/01137 financed by the National Science Center. It also results from the Academic Exchange supported by Narodowa Agencja Wymiany Akademickiej in agreement No. BPN/FRC/2021/1/00003. We also received funding support from the Slovak Scientific Grant Agency VEGA (1/0108/23).

765

766 **References**

767 Abreu, H.S., Latorraca, J.V.F., Pereira, R.P.W., Monteiro, M.B.O., Abreu, F.A., Amparado, K.F., 2009. A
768 supramolecular proposal of lignin structure and its relation with the wood properties. An. Acad.
769 Bras. Cienc. 81, 137–142. https://doi.org/10.1590/s0001-37652009000100014

770 Anupama Jha, Mukul Joshi, Narendra Singh Yadav, Pradeep K. Agarwal, and Bhavanath Jha, 2011.
771 Cloning and characterisation of the Salicornia brachiata Na+/H+ antiporter gene SbNHX1 and its
772 expression by abiotic stress. Mol. Biol. Rep.

773 Barragán, V., Leidi, E.O., Andrés, Z., Rubio, L., de Luca, A., Fernández, J.A., Cubero, B., Pardo, J.M.,
774 2012. Ion exchangers NHX1 and NHX2 mediate active potassium uptake into vacuoles to regulate
775 cell turgor and stomatal function in arabidopsis. Plant Cell 24, 1127–1142.
776 https://doi.org/10.1105/tpc.111.095273

777 Bose, S.K., Francis, R.C., Govender, M., Bush, T., Spark, A., 2009. Bioresource Technology Lignin
778 content versus syringyl to guaiacyl ratio amongst poplars. Bioresour. Technol. 100, 1628–1633.
779 https://doi.org/10.1016/j.biortech.2008.08.046

780 Boughalleb, F., Denden, M., Tiba, B. Ben, 2009. Anatomical changes induced by increasing NaCl salinity
781 in three fodder shrubs, Nitraria retusa, Atriplex halimus and Medicago arborea. Acta Physiol. Plant.
782 31, 947–960. https://doi.org/10.1007/s11738-009-0310-7

783 Cárdenas-Pérez, S., Chanona-Pérez, J.J., Méndez-Méndez, J. V., Calderón-Domínguez, G., López-
784 Santiago, R., Arzate-Vázquez, I., 2016. Nanoindentation study on apple tissue and isolated cells by
785 atomic force microscopy, image and fractal analysis. Innov. Food Sci. Emerg. Technol. 34, 234–242.
786 https://doi.org/10.1016/j.ifset.2016.02.004

787 Cárdenas-Pérez, S., Chanona-Pérez, J.J.J., Güemes-Vera, N., Cybulska, J., Szymanska-Chargot, M.,

788 Chylinska, M., Kozioł, A., Gawkowska, D., Pieczywek, P.M.M., Zdunek, A., 2018. Structural,
789 mechanical and enzymatic study of pectin and cellulose during mango ripening. Carbohydr. Polym.
790 196, 313–321. https://doi.org/10.1016/j.carbpol.2018.05.044

791 Cárdenas-Pérez, S., Niedojadło, K., Mierek-Adamska, A., Dąbrowska, G.B., Piernik, A., 2022. Maternal
792 salinity influences anatomical parameters, pectin content, biochemical and genetic modifications of
793 two Salicornia europaea populations under salt stress. Sci. Rep. 12, 1–16.
794 https://doi.org/10.1038/s41598-022-06385-3

795 Cárdenas-Pérez, S., Piernik, A., Chanona-Pérez, J.J., Grigore, M.N., Perea-Flores, M.J., 2021. An
796 overview of the emerging trends of the Salicornia L. genus as a sustainable crop. Environ. Exp. Bot.
797 191. https://doi.org/10.1016/j.envexpbot.2021.104606

798 Cárdenas-Pérez, S., Piernik, A., Ludwiczak, A., Duszyn, M., Szmidt-Jaworska, A., Chanona-Pérez, J.J.,
799 2020. Image and fractal analysis as a tool for evaluating salinity growth response between two
800 Salicornia europaea populations. BMC Plant Biol. 20. https://doi.org/10.1186/s12870-020-02633-8

801 Chen, X., Bao, H., Guo, J., Jia, W., Tai, F., Nie, L., Jiang, P., Feng, J., Lv, S., Li, Y., 2014. Na+/H+
802 exchanger 1 participates in tobacco disease defence against Phytophthora parasitica var. nicotianae
803 by affecting vacuolar pH and priming the antioxidative system. J. Exp. Bot. 65, 6107–6122.
804 https://doi.org/10.1093/jxb/eru351

805 Chimenti, C.A., Marcantonio, M., Hall, A.J., 2006. Divergent selection for osmotic adjustment results in
806 improved drought tolerance in maise (Zea mays L.) in both early growth and flowering phases. F.
807 Crop. Res. 95, 305–315. https://doi.org/10.1016/j.fcr.2005.04.003

808 Colin, L., Ruhnow, F., Zhu, J.-K., Zhao, C., Zhao, Y., Persson, S., 2023. The cell biology of primary cell
809 walls during salt stress. Plant Cell 35, 201–217. https://doi.org/10.1093/plcell/koac292

810 Debez, A., Saadaoui, D., Ramani, B., Ouerghi, Z., Koyro, H.-W., Huchzermeyer, B., Abdelly, C., 2006.

Leaf H+-ATPase activity and photosynthetic capacity of Cakile maritima under increasing salinity. Environ. Exp. Bot. 3, 285–295. https://doi.org/10.1016/J.ENVEXPBOT.2005.06.009

Dichio, B., Xiloyannis, C., Angelopoulos, K., Nuzzo, V., Bufo, S.A., Celano, G., 2003. Drought-induced variations of water relations parameters in Olea europaea. Plant Soil 257, 381–389. https://doi.org/10.1023/A:1027392831483

Dumitrache, A., Akinosho, H., Rodriguez, M., Meng, X., Yoo, C.G., Natzke, J., Engle, N.L., Sykes, R.W., Tschaplinski, T.J., Muchero, W., Ragauskas, A.J., Davison, B.H., Brown, S.D., 2016. Consolidated bioprocessing of Populus using Clostridium (Ruminiclostridium) thermocellum: A case study on the impact of lignin composition and structure. Biotechnol. Biofuels 9, 1–14. https://doi.org/10.1186/s13068-016-0445-x

Ďurkovič, J., Kačík, F., Husárová, H., Mamoňová, M., Čaňová, I., 2020. Cell wall compositional and vascular traits of hybrid poplar wood in micropropagated plants and plants propagated from root cuttings. New For. 51, 119–135. https://doi.org/10.1007/s11056-019-09723-y

Fan, P., Nie, L., Jiang, P., Feng, J., Lv, S., Chen, X., Bao, H., Guo, J., Tai, F., Wang, J., Jia, W., Li, Y., 2013. Transcriptome analysis of salicornia europaea under saline conditions revealed the adaptive primary metabolic pathways as early events to facilitate salt adaptation. PLoS One 8, 1–20. https://doi.org/10.1371/journal.pone.0080595

Flowers, T.J., Colmer, T.D., 2008. Salinity tolerance in halophytes. New Phytol. 179, 945–963. https://doi.org/10.1111/j.1469-8137.2008.02531.x

Forouzesh, E., Goel, A., MacKenzie, S.A., Turner, J.A., 2013. In vivo extraction of Arabidopsis cell turgor pressure using nanoindentation in conjunction with finite element modeling. Plant J. https://doi.org/10.1111/tpj.12042

Fradera-Soler, M., Grace, O.M., Jørgensen, B., Mravec, J., 2022. Elastic and collapsible: current

understanding of cell walls in succulent plants. J. Exp. Bot. 73, 2290–2307. https://doi.org/10.1093/jxb/erac054

Franceschi, V.R., Horner, H.T., 2014. BOTANICAL 46, 361–427.

Franceschi, V.R., Nakata, P.A., 2005. Calcium oxalate in plants: Formation and function. Annu. Rev. Plant Biol. 56, 41–71. https://doi.org/10.1146/annurev.arplant.56.032604.144106

Grigore, M.-N., Toma, C., 2020. Morphological and Anatomical Adaptations of Halophytes: A Review, Handbook of Halophytes. https://doi.org/10.1007/978-3-030-17854-3_37-1

Hameed, M., Ashraf, M., Naz, N., Al-Qurainy, F., 2010. ANATOMICAL ADAPTATIONS OF CYNODON DACTYLON (L.) PERS., FROM THE SALT RANGE PAKISTAN, TO SALINITY STRESS. I. ROOT AND STEM ANATOMY. Pak. J. Bot 42, 279–289.

Hayatsu, M., Suzuki, S., Hasegawa, A., Tsuchiya, S., Sasamoto, H., 2014. Effect of NaCl on ionic content and distribution in suspension-cultured cells of the halophyte Sonneratia alba versus the glycophyte Oryza sativa. J. Plant Physiol. 171, 1385–1391. https://doi.org/10.1016/j.jplph.2014.06.008

Hessini, K., Martínez, J.P., Gandour, M., Albouchi, A., Soltani, A., Abdelly, C., 2009. Effect of water stress on growth, osmotic adjustment, cell wall elasticity and water-use efficiency in Spartina alterniflora. Environ. Exp. Bot. 67, 312–319. https://doi.org/10.1016/j.envexpbot.2009.06.010

Hori, C., Yu, X., Mortimer, J.C., Sano, R., Matsumoto, T., Kikuchi, J., Demura, T., Ohtani, M., 2020. Impact of abiotic stress on the regulation of cell wall biosynthesis in populus trichocarpa. Plant Biotechnol. 37, 1–11. https://doi.org/10.5511/plantbiotechnology.20.0326a

Hutter, J.L., Bechhoefer, J., 1993. Calibration of atomic-force microscope tips. Rev. Sci. Instrum. 64, 1868–1873. https://doi.org/10.1063/1.1143970

Jaubert-Garibay, S., Hernández-Varela, J.D., Chanona-Pérez, J.J., Cárdenas-Pérez, S., Herrera-López,

E.J., Gutiérrez-López, G.F., 2022. Assessing the product quality of mango slices treated with osmotic and microwave drying by means of image, microstructural, and multivariate analyses. Dry. Technol. 0, 1–15. https://doi.org/10.1080/07373937.2022.2092493

Kačíková, D., Kubovský, I., Ulbriková, N., Kačík, F., 2020. The impact of thermal treatment on structural changes of Teak and iroko wood lignins. Appl. Sci. 10. https://doi.org/10.3390/app10145021

Karadžić, D., Stanivuković, Z., Milanović, S., Sikora, K., Radulović, Z., Račko, V., Kardošová, M., Ďurkovič, J., Milenković, I., 2020. Development of Neonectria punicea Pathogenic Symptoms in Juvenile Fraxinus excelsior Trees. Front. Plant Sci. 11, 1–14. https://doi.org/10.3389/fpls.2020.592260

Kim, J.H., Lee-stadelmann, O.Y., 1984. Water relations and cell wall elasticity quantities in Phaseolus vulgaris leaves. J. Exp. Bot. 35, 841–858. https://doi.org/10.1093/jxb/35.6.841

Koyro, H.W., 2006. Effect of salinity on growth, photosynthesis, water relations and solute composition of the potential cash crop halophyte Plantago coronopus (L.). Environ. Exp. Bot. 56, 136–146. https://doi.org/10.1016/j.envexpbot.2005.02.001

Le Gall, H., Philippe, F., Domon, J.-M., Gillet, O., Rôme Pelloux, J., Rayon, C., 2015. Cell Wall Metabolism in Response to Abiotic Stress 4, 112–166. https://doi.org/10.3390/plants4010112

Li, H., Duijts, K., Pasini, C., Santen, J.E. van, Wang, N., Zeeman, S.C., Santelia, D., Zhang, Y., Testerink, C., 2022. Effective root responses to salinity stress include maintained cell expansion and carbon allocation, bioRxiv. https://doi.org/10.1111/nph.18873

Li, L., Xiao Fei Cheng, Leshkevich, J., Umezawa, T., Harding, S.A., Chiang, V.L., 2001. The last step of syringyl monolignol biosynthesis in angiosperms is regulated by a novel gene encoding sinapyl alcohol dehydrogenase. Plant Cell 13, 1567–1585. https://doi.org/10.1105/tpc.13.7.1567

Liu, J., Shao, Y., Feng, X., Otie, V., Matsuura, A., Irshad, M., Zheng, Y., An, P., 2022. Cell Wall

Components and Extensibility Regulate Root Growth in Suaeda salsa and Spinacia oleracea under salinity. Plants 11, 1–13. https://doi.org/10.3390/plants11070900

Liu, Q., Luo, L., Zheng, L., 2018. Lignins: Biosynthesis and biological functions in plants. Int. J. Mol. Sci. 19. https://doi.org/10.3390/ijms19020335

Lourenço, A., Neiva, D.M., Gominho, J., Curt, M.D., Fernández, J., Marques, A.V., Pereira, H., 2015. Biomass production of four Cynara cardunculus clones and lignin composition analysis. Biomass and Bioenergy 76, 86–95. https://doi.org/10.1016/j.biombioe.2015.03.009

Lu, C., Nianwei, Q., Baoshan, W., Jianhua, Z., 2003. Salinity treatment shows no effects on photosystem IIphotochemistry, but increases the resistance ofphotosystem II to heat stress in halophyteSuaeda salsa_Lu et al 2003.pdf.

Lv, S., Jiang, P., Chen, X., Fan, P., Wang, X., Li, Y., 2012. Multiple compartmentalisation of sodium conferred salt tolerance in Salicornia europaea. Plant Physiol. Biochem. 51, 47–52. https://doi.org/10.1016/j.plaphy.2011.10.015

Marshall, J.G., Dumbroff, E.B., Thatcher, B.J., Martin, B., Rutledge, R.G., Blumwald, E., 1999. Synthesis and oxidative insolubilisation of cell-wall proteins during osmotic stress. Planta 208, 401–408. https://doi.org/10.1007/s004250050575

Martìnez, J.P., Lutts, S., Schanck, A., Bajji, M., Kinet, J.M., 2004. Is osmotic adjustment required for water stress resistance in the Mediterranean shrub Atriplex halimus L? J. Plant Physiol. 161, 1041–1051. https://doi.org/10.1016/j.jplph.2003.12.009

Martínez, J.P., Silva, H., Ledent, J.F., Pinto, M., 2007. Effect of drought stress on the osmotic adjustment, cell wall elasticity and cell volume of six cultivars of common beans (Phaseolus vulgaris L.). Eur. J. Agron. 26, 30–38. https://doi.org/10.1016/j.eja.2006.08.003

Munns, R., Tester, M., 2008. Mechanisms of salinity tolerance. Annu. Rev. Plant Biol. 59, 651–681.

902 https://doi.org/10.1146/annurev.arplant.59.032607.092911

903 Nanowizard, T., n.d. Attaching microspheres to cantilevers using the NanoWizard ® Life Science stage
904 and AFM head Microsphere cantilever tips. Science (80-.). 1–8.

905 Patakas, A., Nikolaou, N., Zioziou, E., Radoglou, K., Noitsakis, B., 2002. The role of organic solute and
906 ion accumulation in osmotic adjustment in drought-stressed grapevines. Plant Sci. 163, 361–367.
907 https://doi.org/10.1016/S0168-9452(02)00140-1

908 Routier-Kierzkowska, A.-L., Weber, a., Kochova, P., Felekis, D., Nelson, B.J., Kuhlemeier, C., Smith,
909 R.S., Technologies, B., Routier-Kierzkowska, A.-L., Weber, a., Kochova, P., Felekis, D., Nelson,
910 B.J., Kuhlemeier, C., Smith, R.S., Technologies, B., 2012. Cellular Force Microscopy for in Vivo
911 Measurements of Plant Tissue Mechanics. Plant Physiol. 158, 1514–1522.
912 https://doi.org/10.1104/pp.111.191460

913 Routier-Kierzkowska, A.L., Smith, R.S., 2013. Measuring the mechanics of morphogenesis. Curr. Opin.
914 Plant Biol. 16, 25–32. https://doi.org/10.1016/j.pbi.2012.11.002

915 Rozentsvet, O., Shuyskaya, E., Bogdanova, E., Nesterov, V., Ivanova, L., 2022. Effect of Salinity on Leaf
916 Functional Traits and Chloroplast Lipids Composition in Two C3 and C4 Chenopodiaceae
917 Halophytes. Plants 11. https://doi.org/10.3390/plants11192461

918 Rui, Y., Dinneny, J.R., 2020. A wall with integrity: surveillance and maintenance of the plant cell wall
919 under stress. New Phytol. 225, 1428–1439. https://doi.org/10.1111/nph.16166

920 Saito, K., Watanabe, Y., Shirakawa, M., Matsushita, Y., Imai, T., Koike, T., Sano, Y., Funada, R.,
921 Fukazawa, K., Fukushima, K., 2012. Direct mapping of morphological distribution of syringyl and
922 guaiacyl lignin in the xylem of maple by time-of-flight secondary ion mass spectrometry. Plant J. 69,
923 542–552. https://doi.org/10.1111/j.1365-313X.2011.04811.x

924 Sánchez-Aguayo, I., Rodríguez-Galán, J.M., García, R., Torreblanca, J., Pardo, J.M., 2004. Salt stress

enhances xylem development and expression of S-adenosyl-L-methionine synthase in lignifying tissues of tomato plants. Planta 220, 278–285. https://doi.org/10.1007/s00425-004-1350-2

Santos, R.B., Capanema, E.A., Balakshin, M.Y., Chang, H.M., Jameel, H., 2012. Lignin structural variation in hardwood species. J. Agric. Food Chem. 60, 4923–4930. https://doi.org/10.1021/jf301276a

Schindelin, J., Arganda-Carreras, I., Frise, E., Kaynig, V., Longair, M., Pietzsch, T., Preibisch, S., Rueden, C., Saalfeld, S., Schmid, B., Tinevez, J.Y., White, D.J., Hartenstein, V., Eliceiri, K., Tomancak, P., Cardona, A., 2012. Fiji: An open-source platform for biological-image analysis. Nat. Methods 9, 676–682. https://doi.org/10.1038/NMETH.2019

Schreiber, S.G., Hacke, U.G., Hamann, A., 2015. Variation of xylem vessel diameters across a climate gradient: Insight from a reciprocal transplant experiment with a widespread boreal tree. Funct. Ecol. 29, 1392–1401. https://doi.org/10.1111/1365-2435.12455

Schuetz, M., Benske, A., Smith, R.A., Watanabe, Y., Tobimatsu, Y., Ralph, J., Demura, T., Ellis, B., Samuels, A.L., 2014. Laccases direct lignification in the discrete secondary cell wall domains of protoxylem. Plant Physiol. 166, 798–807. https://doi.org/10.1104/pp.114.245597

Shi, H., Quintero, F.J., Pardo, J.M., Zhu, J.K., 2002. The putative plasma membrane NA+/H+ antiporter SOS1 controls long-distance NA+ transport in plants. Plant Cell 14, 465–477. https://doi.org/10.1105/tpc.010371

Sluiter, A., Ruiz, R., Scarlata, C., Sluiter, J., Templeton, D., 2008. Determination of Extractives in Biomass: Laboratory Analytical Procedure (LAP); Issue Date 7/17/2005.

Soil salinity | Global Soil Partnership | Food and Agriculture Organization of the United Nations [WWW Document], n.d. URL https://www.fao.org/global-soil-partnership/areas-of-work/soil-salinity/en/ (accessed 1.27.23).

948 Solis, C.A., Yong, M.T., Zhou, M., Venkataraman, G., Shabala, L., Holford, P., Shabala, S., Chen, Z.H.,
949 2022. Evolutionary Significance of NHX Family and NHX1 in Salinity Stress Adaptation in the
950 Genus Oryza. Int. J. Mol. Sci. 23, 1–25. https://doi.org/10.3390/ijms23042092

951 Tenhaken, R., 2015. Cell wall remodeling under abiotic stress. Front. Plant Sci. 5, 1–9.
952 https://doi.org/10.3389/fpls.2014.00771

953 Tester, M., Davenport, R., 2003. Na+ tolerance and Na+ transport in higher plants. Ann. Bot. 91, 503–
954 527. https://doi.org/10.1093/aob/mcg058

955 Tooulakou, G., Giannopoulos, A., Nikolopoulos, D., Bresta, P., Dotsika, E., Orkoula, M.G., Christos, G.,
956 Fasseas, C., Liakopoulos, G., Klapa, M.I., Tooulakou, G., Giannopoulos, A., Nikolopoulos, D.,
957 Bresta, P., Dotsika, E., Orkoula, M.G., Kontoyannis, C.G., Liakopoulos, G., Klapa, M.I.,
958 Karabourniotis, G., 2016. Reevaluation of the plant " gemstones ": Calcium oxalate crystals sustain
959 photosynthesis under drought conditions. Plant Signal. Behav. 11, 1–4.
960 https://doi.org/10.1080/15592324.2016.1215793

961 Xiao, X., Ma, J., Wang, J., Wu, X., Li, P., Yao, Y., 2015. Validation of suitable reference genes for gene
962 expression analysis in the halophyte salicornia europaea by real-time quantitative pcr. Front. Plant
963 Sci. https://doi.org/10.3389/fpls.2014.00788

964 Xiong, L., Zhu, J.-K., 2002. Salt Tolerance. Arab. B. 1, e0048. https://doi.org/10.1199/tab.0048

965 Yadav, N.S., Shukla, P.S., Jha, A., Agarwal, P.K., Jha, B., 2012. The SbSOS1 gene from the extreme
966 halophyte Salicornia brachiata enhances Na+loading in xylem and confers salt tolerance in
967 transgenic tobacco. BMC Plant Biol. 12, 1. https://doi.org/10.1186/1471-2229-12-188

968 Yang, X., Ji, J., Wang, G., Yang, S., Zhao, Q., Josine, T.L., 2011. Over-expressing Salicornia europaea
969 (SeNHX1) gene in tobacco improves tolerance to salt. African J. Biotechnol. 10, 16452–16460.
970 https://doi.org/10.5897/AJB11.1092

971 Yoo, C.G., Dumitrache, A., Muchero, W., Natzke, J., Akinosho, H., Li, M., Sykes, R.W., Brown, S.D.,
972 Davison, B., Tuskan, G.A., Pu, Y., Ragauskas, A.J., 2018. Significance of Lignin S/G Ratio in
973 Biomass Recalcitrance of Populus trichocarpa Variants for Bioethanol Production. ACS Sustain.
974 Chem. Eng. 6, 2162–2168. https://doi.org/10.1021/acssuschemeng.7b03586

975 Zdunek, A., Kurenda, A., 2013. Determination of the elastic properties of tomato fruit cells with an atomic
976 force microscope. Sensors (Basel). 13, 12175–12191. https://doi.org/10.3390/s130912175

977 Zörb, C., Mühling, K.H., Kutschera, U., Geilfus, C.M., 2015. Salinity stiffens the epidermal cell walls of
978 salt-stressed maise leaves: Is the epidermis growth-restricting? PLoS One 10, 1–15.
979 https://doi.org/10.1371/journal.pone.0118406

980